Liquefied microcapsules compartmentalizing macrophages and umbilical cord-derived cells for bone tissue engineering

Sara Nadine, Inês Fernandes, Sónia G. Patrício, Clara R. Correia, João F. Mano**

S. Nadine, I. Fernandes, Dr. S. G. Patrício, Dr. C. R. Correia, Prof. J. F. Mano
CICECO – Aveiro Institute of Materials, Department of Chemistry, University of Aveiro, Campus Universitário de Santiago, 3810-193 Aveiro, Portugal
E-mail: claracorreia@ua.pt and jmano@ua.pt

Keywords: osteoimmunomodulation; liquefied microcapsules; macrophages; umbilical cord-derived cells; biomimetic bone niches; electrohydrodynamic atomization; dynamic cultures

Extraordinary capabilities underlie the potential use of immune cells, particularly macrophages, in bone tissue engineering. Indeed, the depletion of macrophages during bone repair often culminates in disease scenarios. Inspired by the native dynamics between immune and skeletal systems, this work proposes a straightforward in vitro method to bioengineer biomimetic bone niches using biological waste. For that, liquefied and semipermeable reservoirs generated by electrohydrodynamic atomization and layer-by-layer techniques are developed to coculture umbilical cord‐derived human cells, namely monocyte‐derived macrophages, mesenchymal-derived stromal cells (MSCs), and human umbilical vein endothelial cells (HUVECs). Poly(ε-caprolactone) microparticles are also added to the liquefied core to act as cell carriers. The fabricated microcapsules grant the successful development of viable microtissues, ensuring the high diffusion of bioactive factors. Interestingly, macrophages within the bioengineered microcapsules increase the release of osteocalcin, osteoprotegerin, and vascular endothelial growth factor. The cytokines profile variation indicates macrophages' polarization into a prohealing phenotype. Altogether, the incorporation of macrophages within the fabricated microcapsules allows to recreate an appropriate bone microenvironment for developing new bone mineralized microtissues. The proposed bioencapsulation protocol is a powerful self‐regulated system, which might find great applicability in bone tissue engineering based on bottom‐up approaches or disease modeling.

1. Introduction

The well-known interaction between immune cells and native niches changed the tissue engineering and regenerative medicine paradigm. Nowadays, biomaterials are designed to modulate immune cells and the microenvironment upon implantation instead of avoiding an immune response.[1] The immune system plays an indispensable regulatory role during the different stages of development, remodeling, and regeneration of bone tissue.[2,3] Among the different immune cells, macrophages have been under the spotlight during the last years.[4] Besides their known role in initiating inflammation and clearing the tissue debris, macrophages are essential for bone homeostasis and have an active function during intramembranous and endochondral ossification.[5,6] After a fracture, macrophages participate in the healing process by secreting pro-regenerative cytokines, supporting mesenchymal stromal cells (MSCs)-mediated bone formation, and facilitating angiogenesis.[7] In fact, the cell-to-cell contact between MSCs/osteoblasts and macrophages is essential in regulating and promoting osteogenic differentiation.[8–10] Besides, MSCs also immunomodulate the macrophage behavior by turning them less inflammatory.[11] The depletion of macrophages during fracture repair leads to failure in bone mineralization *in vivo*.[5,12] Importantly, the encapsulation of macrophages in hydrogels can influence the incoming host's cell behavior, being able to facilitate the integration of biomaterial upon implantation.[13] Considering such statements, it is crucial to incorporate the osteoimmunomodulation concept when fabricating new bone biomaterials.[14]

The crosstalk between osteoblastic and endothelial cells has also proven necessary to promote osteogenic and angiogenic differentiation and improve the survival of engineered constructs.[15–18] During bone repair, osteoprogenitor cells release biomolecules involved in the recruitment and proliferation of endothelial cells, while endothelial cells release numerous osteogenic factors that support the differentiation and activity of osteoblasts.[19,20] In fact, bone is a highly vascularized tissue that presents a complex and dynamic environment, encompassing multiple cell phenotypes, biochemical and physical signals, and extrinsic mechanical forces.[21] Therefore, the development of an efficient and reproducible bone tissue engineering strategy often depends on achieving a balance between complexity and functionality, where lessons from bone physiology have been particularly useful.[21]

Considering the importance of cellular balance and macrophages during bone lifetime, we developed an *in vitro* bioencapsulation system to fabricate bone niches inspired by the native dynamics between immune and skeletal systems. The concept is established on the co-culture of umbilical cord-derived cells, namely monocyte-derived macrophages, Wharton's jelly's MSCs, and human umbilical vein endothelial cells (HUVECs), within liquefied semipermeable miniaturized reservoirs designed to drive self-regulated osteogenesis. The aim is to develop a

straightforward protocol to mimic the bone microenvironment within the well-established liquefied microcapsules and create bone-like mineralized microtissues.[18,22–26]

Inspired by such a concept, firstly, microgels containing the cells mentioned above and surface-functionalized poly(ε-caprolactone) (PCL) microparticles were generated by electrohydrodynamic atomization. Then, the microgels were surrounded by a multilayered membrane obtained through the layer-by-layer assembly of poly(L-lysine), alginate, and chitosan. The created membrane is permeable to nutrients, oxygen, and metabolites and avoids the dispersion of the microcapsules content. Ultimately, the core was liquefied by chelation utilizing ethylenediaminetetraacetic acid (EDTA). The liquefied core permits the effortless diffusion of small biomolecules while cells can freely move within the miniaturized compartmentalized area. Moreover, the microparticles provide cell adhesion sites within the liquefied environment, allowing anchorage-dependent cells to adhere, proliferate, and recruit other cells and microparticles according to their needs. The microcapsules were dynamically tested in spinner flasks to simulate the active environment of native bone tissue. We have previously confirmed that the biophysical stimulation provided to microcapsules upregulates osteogenic differentiation and bone mineralization.[25] The fabrication and content of the biomimetic bone niches are represented in **Scheme 1**.

Herein, we propose a method to bioengineer biomimetic bone niches utilizing human cells recovered from the umbilical cord tissue and blood. Harvesting cells from the umbilical cord tissue and blood quickly became attractive due to their ease of isolation, cell availability, immunocompatibility, and no donor site morbidity.[27] Thus, collecting and banking umbilical cord-derived cells after delivery has become a trendy procedure; otherwise, they would be discarded as biological waste.[28] An advantage of utilizing autologous umbilical cord cells for regenerative purposes is avoiding immune rejection complications. Besides, umbilical cord-derived MSCs are hypoimmunogenic, which means that the host's immune system will tolerate allogeneic transplantation.[29,30] MSCs isolated from the umbilical cord's Wharton's jelly are highly proliferative, less heterogeneous than adult MSCs, and present multilineage differentiation potential.[31,32] HUVECs have also been widely explored as a tool in order to create vascular networks in 3-dimensional (3D) bone constructs.[33,34] The umbilical cord blood is an excellent source of immune cells, including monocytes, which, after *in vitro* differentiation into macrophages, were shown to improve osteoblastic maturation.[35]

In the current study, liquified microcapsules encapsulating a co-culture of MSCs and HUVECs, with (TRI microcapsules) or without (CO microcapsules) monocyte-derived macrophages were cultured for 21 days in basal or osteogenic differentiation media. The main goal is to promote a well-orchestrated cell-to-cell interaction enabling the evaluation of the bioperformance of

macrophages toward bone regeneration. Moreover, the liquefied microcapsules are intended to be injected *in situ* by minimally invasive procedures for bone tissue engineering applications or to be used as individual units for post-assembling or bioprinting, using bottom-up tissue engineering approaches.[36] We envision modulating the local immune environment while inducing bone regeneration, angiogenesis, and osteointegration.

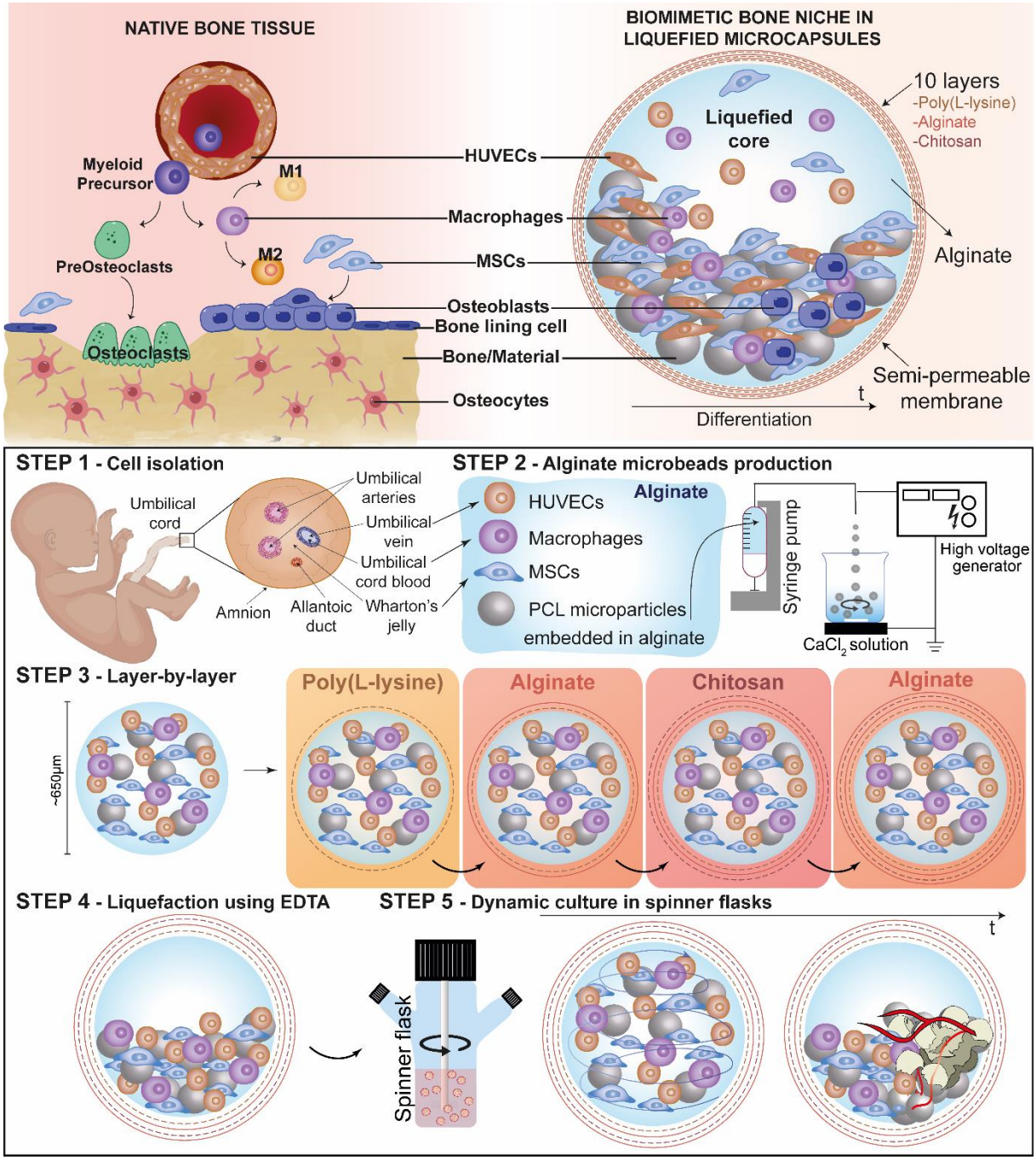

Scheme 1. Fabrication of a biomimetic bone niche using liquefied microcapsules. Schematics comparing the cellular components between the native bone tissue and the bone-engineered niche developed inside liquefied microcapsules. Microcapsules production: Step 1 - MSCs and HUVECs were isolated from Wharton's jelly and umbilical vein, respectively. Monocytes were isolated from the umbilical cord blood and then differentiated into macrophages. Step 2 - To

produce microgels, cells and PCL microparticles were embedded in alginate. Microgels were generated by electrohydrodynamic atomization. Step 3 - After obtaining microgels encapsulating cells and microparticles, a 10-layered membrane was fabricated applying the layer-by-layer technique, using poly(L-lysine), alginate, and chitosan as polyelectrolytes. Step 4 - The alginate core was liquefied by chelation using EDTA. Step 5 - Liquefied microcapsules were cultured in spinner flasks. The confined biomolecular interactions inside the microcapsules are expected to recreate the bone repair process, namely with calcification and vasculature organization.

2. Results

2.1. Cell isolation and fabrication of liquefied microcapsules

After isolation of MSCs, HUVECs, and monocytes from the umbilical cord tissue and blood, their phenotypic characterization was determined by flow cytometry. MSCs did not express the endothelial and hematopoietic lineage markers CD31 and CD34 and were positive for CD73, CD90, and CD105 (Figure S1a - Supporting Information). More than 95% of HUVECs were positive for CD31 and negative for CD34 (Figure S1b - Supporting Information). The success rate of monocytes isolation from the umbilical cord blood utilizing a CD14 positive immunomagnetic separation kit was approximately 95% (Figure S1c - Supporting Information). The isolated monocytes were differentiated into macrophages by adding macrophage stimulation factor (M-CSF). The non-polarized macrophages were positive for CD16, CD197, and CD206 without expressing the CD80 and CD163 phenotypic markers (Figure S1d - Supporting Information). Then, MSCs and HUVECs were co-cultured with (TRI microcapsules) or without (CO microcapsules) non-polarized macrophages within the liquefied microcapsules containing PCL microparticles. The microparticles generated by the emulsion solvent evaporation technique presented a diameter of 49.64 ± 6.25 μm (**Figure 1a**). Afterward, the fabrication of microcapsules was successfully achieved by electrohydrodynamic atomization. The diameter of the obtained microcapsules was 649.5 ± 87.14 μm (**Figure 1b**). After 7 days of culture, it was possible to observe aggregates of cells and microparticles surrounded by the multilayered membrane dyed in blue (**Figure 1c**). Moreover, the presence of different cell phenotypes and their random distribution following encapsulation were confirmed by microscopic analysis. MSCs (DiO - green), HUVECs (DiD - pink), and macrophages (Dil - orange) were stained with lipophilic dyes before encapsulation and analyzed after 1 and 7 days of culture (**Figure 1d**). Besides the expected interaction of MSCs and HUVECs, macrophages were also involved in the formation of aggregates, as observed after 7 days of TRI

microcapsules culture. The average size of the developed aggregates of cells and microparticles at the last time-point was 217.43 ± 33.98 μm.

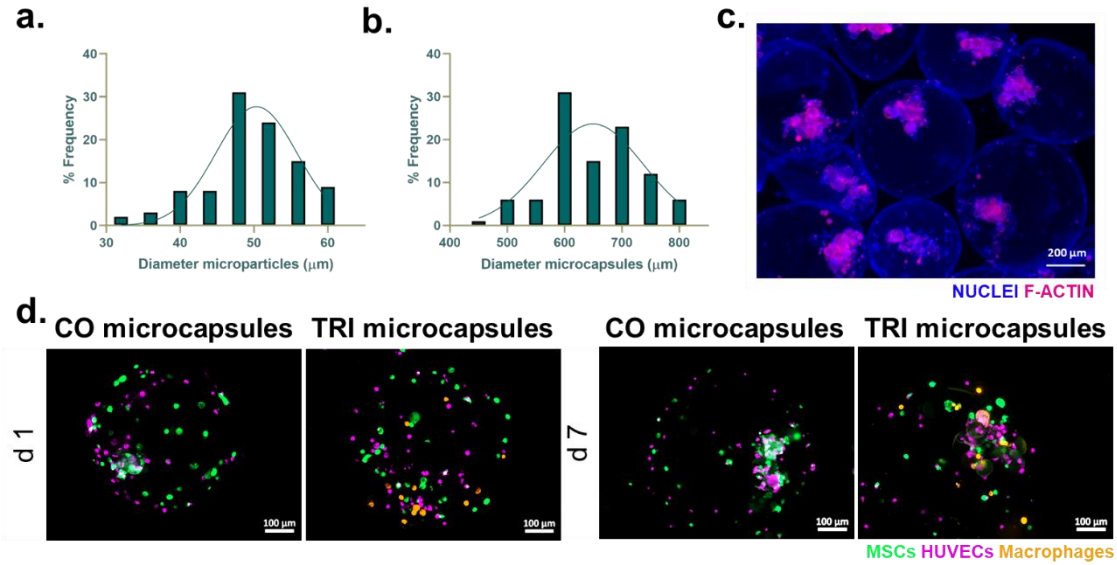

Figure 1. Production of liquefied microcapsules. Size distribution histogram (n=100) of (a) PCL microparticles and (b) liquefied microcapsules. (c) Fluorescence microscopy image depicting microcapsules membrane and cell nuclei with DAPI (blue) after 7 days of culture. Actin filaments were stained with phalloidin (pink). (d) Fluorescence microscopy images reveal cells' spatial distribution inside CO and TRI microcapsules on days 1 and 7 of culture in basal medium. The encapsulated cells were previously labeled with DiO (MSCs, green), DiD (HUVECs, pink), and Dil (macrophages, orange) lipophilic fluorescent dyes.

2.2. Cellular response of encapsulated content

The potential of the proposed encapsulation system for long-term cell survival was demonstrated through a Live-Dead fluorescence assay. The microscopic images show that cells adhered to the microparticles and remained viable during the 21 days of culture for both CO and TRI microcapsules (**Figure 2a**). The metabolic activity evaluated by MTS colorimetric assay also increased over time, mainly for osteogenic cultures and microcapsules containing

macrophages (**Figure 2b**). After 21 days of culture, it was possible to observe the new matrix deposited by cells, fully covering the microparticles (**Figure 2d**).

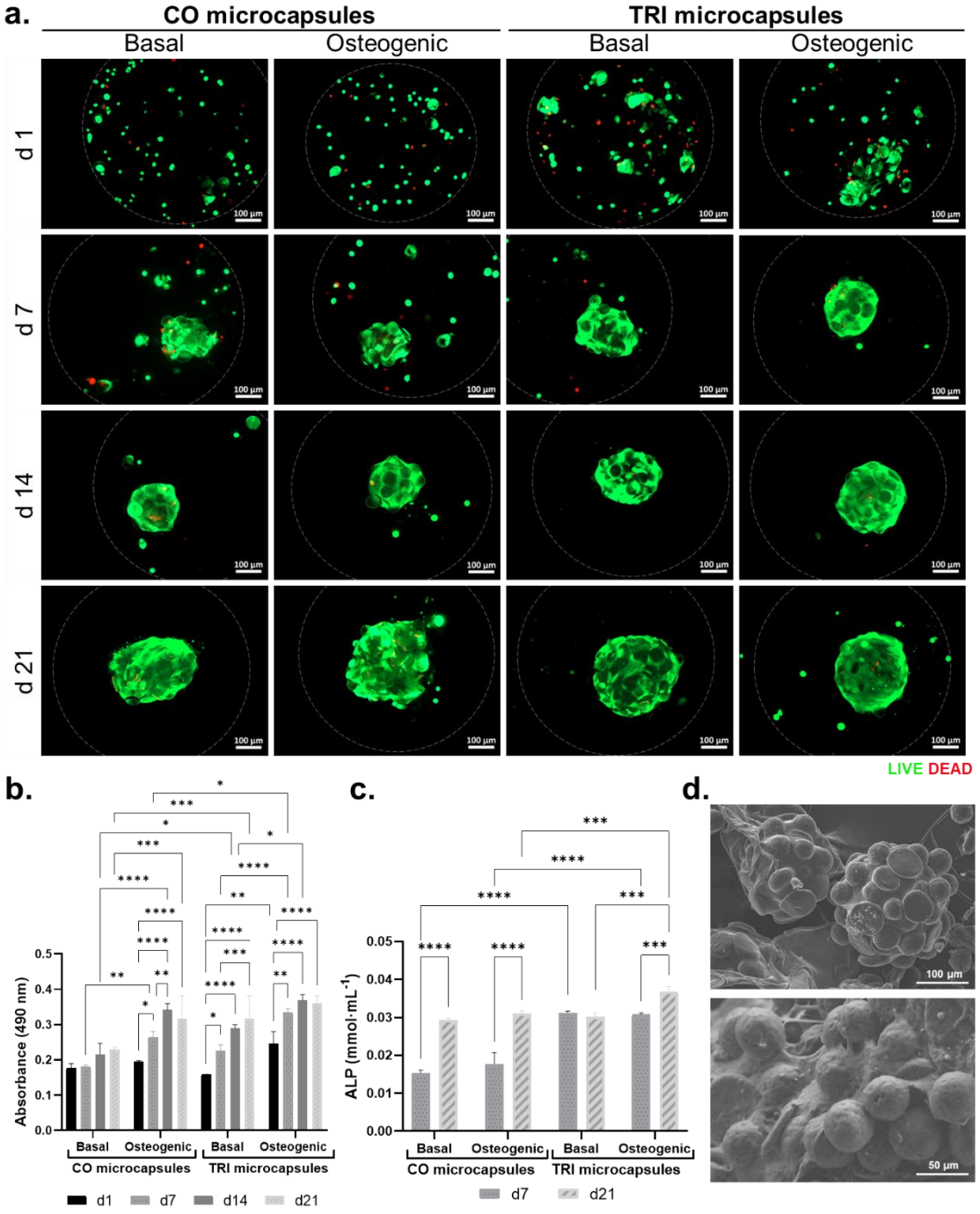

Figure 2. Cellular response of microcapsules cultured in basal and osteogenic media for 21 days. (a) Live-Dead analysis of CO and TRI microcapsules. Live cells were stained with calcein-AM (green) and dead cells with ethidium homodimer-1 (red). Dotted lines correspond to the polymeric permselective membrane of microcapsules. (b) Cellular metabolic activity evaluation of microcapsules by colorimetric MTS assay at 1, 7, 14, and 21 days of culture (n=4). (c) ALP activity of microcapsules on days 7 and 21 of culture (n=4). *p*-values<0.05 were

considered statistically significant (****p<0.0001; ***p<0.001; **p<0.01; *p<0.05). (d) Scanning electron microscopy images of microcapsules' content show the formation of aggregates of cells and microparticles, as well as the deposition of the extracellular matrix after 21 days of culture. Magnification corresponds to 250x and 500x for the top and bottom images, respectively.

2.3. Osteogenic potential of liquefied microcapsules

The alkaline phosphatase (ALP) activity, an enzyme associated with bone mineralization[37], was evaluated after 7 and 21 days of culture. Results show that the ALP activity significantly increased over time for all conditions, except for TRI microcapsules cultured in basal medium (**Figure 2c**). Interestingly, the presence of macrophages within microcapsules significantly enhanced the ALP activity compared to CO microcapsules, with more emphasis after 7 days of culture. The immunofluorescence staining of osteopontin (OPN) and osteocalcin (OCN) was also evaluated after 21 days post-encapsulation. While the late osteogenic marker OPN was expressed in all conditions (**Figure 3a**), OCN, which is solely secreted by osteoblasts[38], was mainly expressed by TRI microcapsules (**Figure 3b** and Figure S2d - Supporting Information). The presence of macrophages promoted OCN secretion even without supplementation with osteogenic differentiation factors. In the co-culture system, we can observe a slight expression of OCN when supplemented with osteogenic factors.

The release of OPN, osteoprotegerin (OPG), and bone morphogenetic protein 2 (BMP-2) was measured utilizing the LegendPLEX kit after 21 days post-encapsulation. The release of OPN was significantly higher in TRI microcapsules cultured in basal medium (**Figure 3c**). On the other hand, the release of the protein OPG, which is involved in the regulation of osteoclastogenesis[39], was also enhanced in microcapsules containing macrophages, with a statistical significance for microcapsules cultured in osteogenic medium (**Figure 3d**). The supplementation with osteogenic medium or the presence of macrophages enhanced the release of BMP-2 (**Figure 3e**), which is essential for fracture healing.[40] The release of OPN, OPG, and BMP-2 was also detected after 7 days o culture. Although there are no significant

differences between conditions, it was possible to observe an increase in the protein released by microcapsules between days 7 and 21 (Figure S2a-c - Supporting Information).

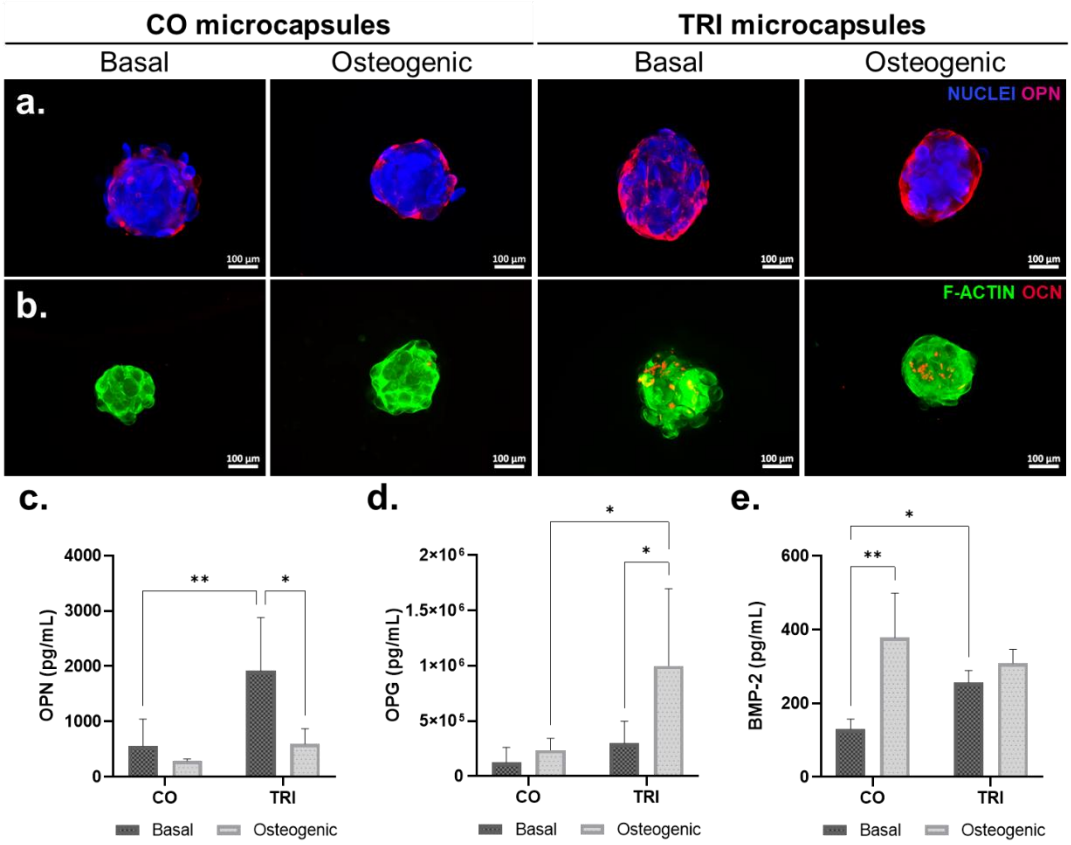

Figure 3. Osteogenic differentiation capacity of microcapsules cultured in basal and osteogenic media for 21 days. (a) Immunofluorescence of OPN (red) in CO and TRI microcapsules. Actin filaments were counterstained with phalloidin (green). (b) Immunofluorescence of OCN (pink) in CO and TRI microcapsules. Cell nuclei were counterstained with DAPI (blue). (c-e) Quantification of OPN, OPG, and BMP-2 measured by LegendPLEX Human Bone Metabolism Panel (n=4). *p*-values<0.05 were considered statistically significant (****p<0.0001; ***p<0.001; **p<0.01; *p<0.05).

2.4. Matrix mineralization evaluation

The existence of mineralization was confirmed by scanning electron microscopy coupled with energy-dispersive x-ray spectroscopy (SEM-EDS). After 21 days of culture, the microscopic images revealed the presence of crystals in all formulations (**Figure 4a**). Then, the developed microtissues were characterized regarding their content in phosphorous (P) and calcium (Ca). Although all conditions presented high levels of P and Ca, CO and TRI microcapsules cultured in osteogenic medium developed microtissues fully enriched in minerals. Additionally, the

distribution of P (green) and Ca (red) was exhibited by chemical mapping, with the overlap of both elements represented in yellow. These results were only visualized after cutting the aggregates in half. There are no significant differences between conditions by analyzing the Ca/P ratio of microtissues (**Figure 4b**). In fact, the developed hydroxyapatite-like minerals presented Ca/P ratios around 1.75, which are analogous to the native hydroxyapatite.[41] The fluorescent staining of hydroxyapatite nodules utilizing the OsteoImage Mineralization Assay Kit was similar between conditions. After 21 days, CO and TRI microcapsules cultured in basal and osteogenic media exhibited a similar amount of hydroxyapatite nodules (green) embedded in the extracellular matrix (**Figure 4c** and Figure S2e - Supporting Information).

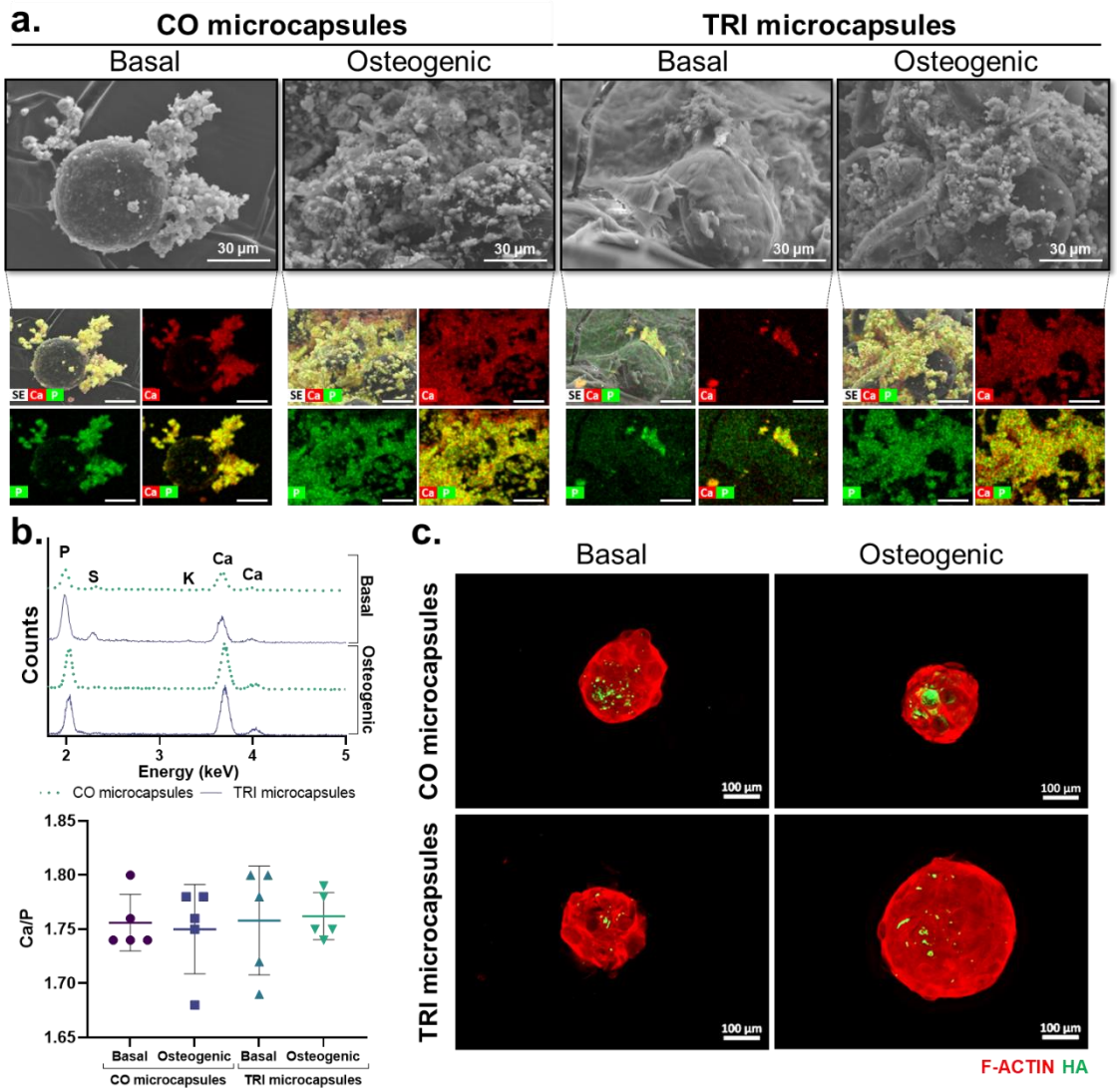

Figure 4. Skeletal extracellular matrix mineralization of CO and TRI microcapsules cultured in basal and osteogenic media for 21 days. (a) Scanning electron microscopy images of encapsulated cells and microparticles and corresponding elemental analysis by chemical mapping of phosphorous (P, red) and calcium (Ca, green). Scale bars correspond to 30 µm. (b) Identification of chemical elements by energy-dispersive x-ray spectroscopy and Ca/P ratio

analysis of microcapsules' content spot sizes (n=5). (c) Hydroxyapatite accumulation (green) was assessed utilizing the OsteoImage Mineralization Assay Kit. Actin filaments were counterstained with phalloidin (red).

2.5. Angiogenic and immunomodulatory capability of liquefied microcapsules

The immunofluorescence staining of CD31 allowed to localize HUVECs in the *in vitro* microtissues after 21 days of culture. Most of the endothelial cells (stained green) were found in the inner part of the microtissues (**Figure 5a**). The internal location of endothelial cells had been previously observed in another study using liquefied capsules.[18] Afterward, the release of vascular endothelial growth factor (VEGF) was detected by enzyme-linked immunosorbent assay (ELISA). Remarkably, the release of this potent angiogenic factor was significantly higher when macrophages were encapsulated in microcapsules (**Figure 5b**). Moreover, the pro-angiogenic potential of microcapsules was evaluated utilizing an endothelial tube formation assay. The supernatants of TRI microcapsules increased the capillary-like structures of HUVECs *in vitro* (**Figure 5c** and Figure S3 – Supporting Information). In fact, the number of meshes, junctions, segments, and total segment length was significantly higher in the presence of macrophages (**Figure 5d**). However, no differences were noticed between microcapsules cultured in basal and osteogenic media.

Ultimately, we analyzed a LegendPLEX Human M1/M2 Macrophage Panel to evaluate the polarization of macrophages and the immunomodulatory ability of microcapsules over time. The quantification of cytokines was measured in the culture medium without destroying the microcapsules since the multilayered membrane allows the diffusion of small biomolecules. The pro-inflammatory cytokine IL-6 significantly decreased over time for all conditions, except for CO microcapsules cultured in osteogenic medium, in which the decrease was not statistically significant (**Figure 6a**). Tumor necrosis factor α (TNF-α) and IL-1β were also two pro-inflammatory mediators analyzed in the medium. TNF-α was only significantly higher for CO microcapsules after 7 days of culture in basal medium; otherwise, the released amount was constant (**Figure 6b**). TRI microcapsules cultured in osteogenic medium released a higher amount of IL-1β compared to other conditions (**Figure 6c**); however, this quantity significantly decreased after 21 days of culture. On the other hand, the release of the anti-inflammatory/pro-regenerative cytokines, IL-10, and IL-1 receptor antagonist (IL-1RA) was higher in microcapsules encapsulating macrophages. After 21 days of culture, the release of IL-10 was significantly higher in TRI microcapsules cultured in the osteogenic medium (**Figure 6d**). Furthermore, the IL-10 amount also increased compared to day 7 for the same condition. The secretion of IL-1RA was superior for TRI microcapsules, with a statistical difference on day 7

(**Figure 6e**). The IL-6/IL-10 ratio was calculated to evaluate the balance between a pro- versus an anti-inflammatory environment. Results show that the IL-6/IL-10 ratio decreased over time for all conditions, with statistical significance for CO microcapsules cultured in basal medium and TRI microcapsules cultured in osteogenic medium (**Figure 6f**). Decreased IL-6/IL-10 ratio is usually associated with better regenerative outcomes after tissue damage.[42]

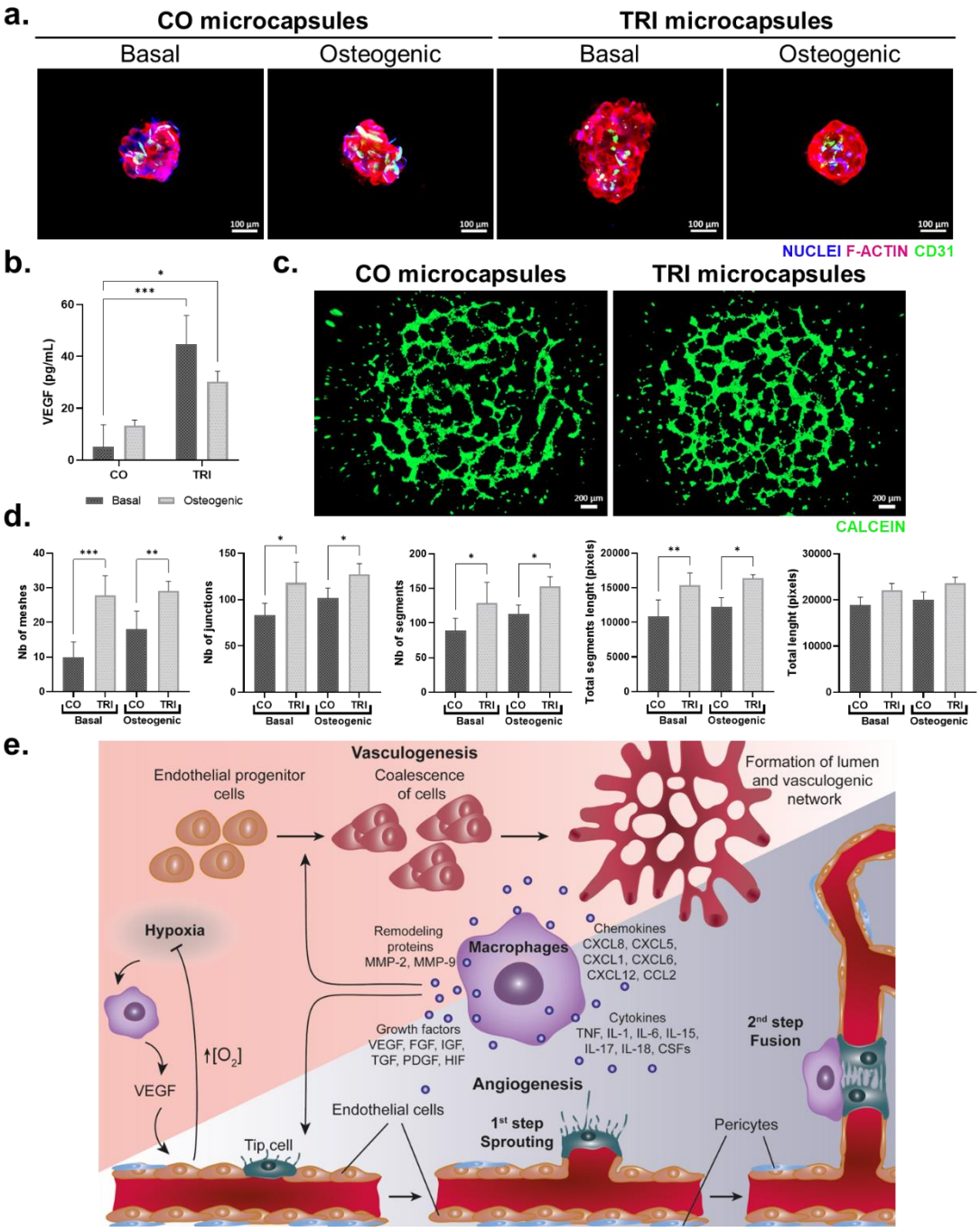

Figure 5. Analysis of the angiogenic potential of CO and TRI microcapsules cultured in basal and osteogenic media for 21 days. (a) Immunofluorescence of CD31 (green) in CO and TRI microcapsules. Actin filaments and nuclei were counterstained with phalloidin (pink) and DAPI

(blue), respectively. (b) Quantification of VEGF release by ELISA (n=4). (c) Representative microscopic images of the endothelial tube formation assay incubated with supernatants of microcapsules (osteogenic condition). (d) Tube formation was analyzed using the ImageJ software with the Angiogenesis Analyzer plugin to quantify the number of meshes, junctions, and segments and the total segment length and total length (n=5). *p*-values<0.05 were considered statistically significant (****p<0.0001; ***p<0.001; **p<0.01; *p<0.05). (e) Role of macrophages during angiogenesis and vasculogenesis.

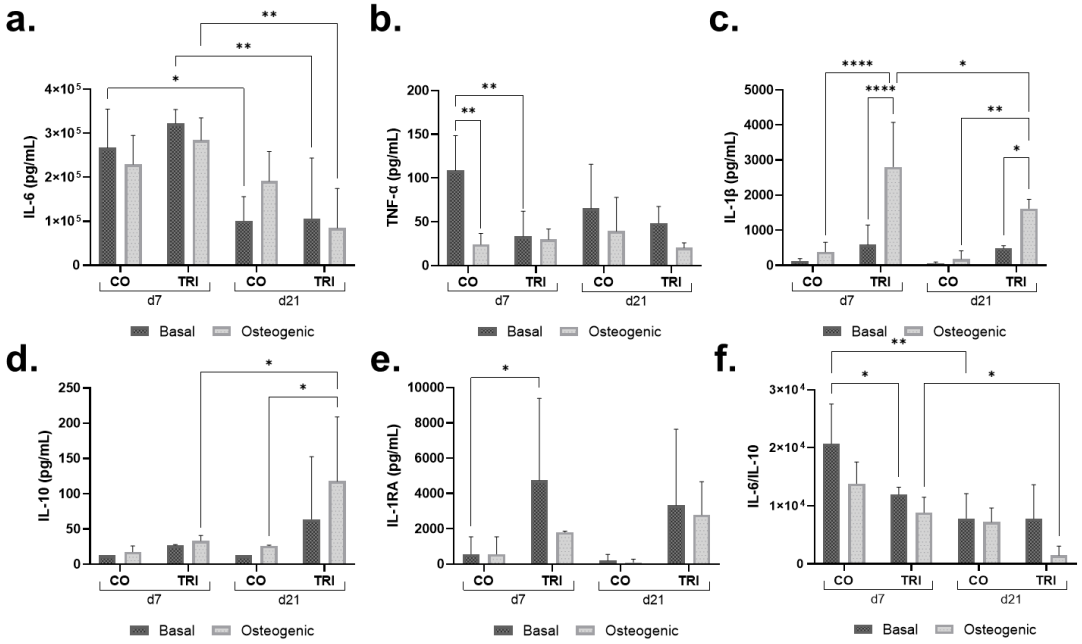

Figure 6. Immunomodulatory analysis of CO and TRI microcapsules cultured in basal and osteogenic media for 21 days (n=4). Quantification of the release of (a-c) pro-inflammatory (IL-6, TNF-α, and IL-1β) and (d-e) anti-inflammatory (IL-10 and IL-1RA) cytokines measured by LegendPLEX Human M1/M2 Macrophage Panel. (f) IL-6/IL-10 ratio evaluation. *p*-values<0.05 were considered statistically significant (****p<0.0001; ***p<0.001; **p<0.01; *p<0.05).

3. Discussion

Different tissue engineering constructs have been proposed in an effort to find the best bone replacement strategy.[43] Among the numerous bottom-up approaches, hydrogels are being widely explored due to their resemblance with the native extracellular matrix, water content, and cell compatibility.[44] However, common limitations related to the lack of mechanical strength, necrosis at the bulk of hydrogels, and inadequate diffusion of oxygen and nutrients prompted us to develop liquefied and multilayered microcapsules.[18,22–26] Liquefied

microcapsules offer unique advantages compared to other hydrogels by presenting better diffusion of essential biomolecules for long-term cell survival and holding particles that act as physical support for cell adhesion. The liquefied environment provides freedom for the encapsulated cells to self-construct in a 3D fashion according to their specific needs. Additionally, the crosslinking degree of other cell-laden strategies decreases the diffusion coefficient of water and small solutes, and usually, most hydrogels require modification of the polymeric matrix to enhance their cell adhesive properties since most cells are anchorage-dependent.[45,46] As demonstrated in the Live-Dead assay, most cells remained adhered to microparticles and alive after 21 days in culture (**Figure 2a**). Both MSCs, HUVECs, and macrophages were shown to attach to the microparticles generating aggregates after 7 days of culture (**Figure 1d**). Although we observed good cell viability, increased metabolic activity, and larger aggregates of cells and microcapsules over time, which means that cells were proliferating, the DNA quantity did not increase (Figure S4 – Supporting Information). Similar results were observed in the MTS assay in the last time-points. We presume that this issue is related to difficulties in optimizing the protocol for destroying microaggregates composed of cells and microparticles. Besides the ability to create capsules of different sizes, from micro- to macro-scales, we can generate liquefied capsules with different geometries, including circles, squares, and cylinders.[26,47] Additionally, it is possible to take advantage of the liquefied environment and culture the microcapsules in dynamic systems, where cells and microparticles can freely move inside the compartmentalized reservoir and build their 3D cell culture assembly system. We previously observed that the fluid flow promoted by spinner flasks, which mimics the dynamic microenvironment of bone, increased osteogenesis and mineralization of the developed bone-like microtissues within microcapsules.[25] Additionally, only 1 day of culture, the dynamic flow allowed the recruitment of almost all cells and microparticles, while in static conditions, the microcapsules content was completely dispersed. Utimately, the structural analysis of the collagen-rich extracellular matrix was also evaluated by Fourier transform infrared spectroscopy – attenuated total reflectance (FTIR-ATR) through the deconvolution of the amide I band in the 1700–1600 cm^{-1} range. Interestingly, the mechanical stimulation added to the microcapsules enhanced the complexity of the deposited collagen compared to static conditions.[25] Moreover, larger aggregates can be obtained in liquefied systems compared to crosslinked ones. The average size of the developed aggregates after 21 days of culture was 217.43 ± 33.98 μm. Also, after 7 days of culture, most cells were attached to microparticles and developed a single aggregate within the confined system. Compared to alginate crosslinked beads in similar conditions, after 7 days of culture, there is usually still a distance between

cells.[48,49] Thus, at early times of culture, we would expect a faster development of microtissues in liquefied encapsulation systems.

Thus, in order to generate an *in vitro* biomimetic bone niche inspired by the native dynamics between immune and skeletal systems, we proposed the encapsulation of MSCs, HUVECs, and macrophages in liquefied microcapsules. We aimed to promote a well-orchestrated cell-to-cell interaction within the liquefied reservoirs to drive self-regulated osteogenesis. Additionally, we could evaluate the role of macrophages during the generation of bone-like microtissues within our encapsulation system. Juhas and colleagues proposed a great example of bridging the immune system and tissue engineering by incorporating macrophages in 3D muscle constructs. Results demonstrated that macrophages stimulated the myogenesis of muscle satellite cells *in vitro* while increasing the blood vessel ingrowth, muscle regeneration, and contractile function *in vivo*.[50] The contradictory findings on the influence of macrophages on osteogenesis are a reality that the scientific community has to deal with, and it proves that there is still much research to do.[51,52] The co-culture of stromal and endothelial cells was already evaluated inside the encapsulation system *in vitro* and *in vivo*.[17,18] However, these studies utilized stromal and endothelial cells obtained from liposuction procedures encapsulated in larger capsules (ca. 1.8 mm in diameter) under static culture systems. Data showed that osteogenesis and mineralization were enhanced in the presence of endothelial cells. Such results are in agreement with the literature, which states that there is a synergistic interplay between osteoprogenitor and endothelial cells during the different phases of bone life.[15–18] Therefore, incorporating endothelial cells in 3D engineered constructs has been rising to solve issues related to insufficient blood supply following implantation. In contrast, there has been little research in the tissue engineering industry targeting macrophages or the crosstalk between macrophages and MSCs to improve bone regeneration. There is factual evidence that macrophages play fundamental regulatory roles in essential aspects of the bone healing process. Macrophages secrete pro-inflammatory cytokines (TNF-α, IL-6, IL-1β, IFN-γ, and oncostatin M) that were shown to stimulate osteogenic differentiation. The direct cell-cell contact between macrophages and MSCs leads to the production of oncostatin M, which induces signal transducer and activator of transcription 3 (STAT3) phosphorylation and MSCs differentiation into osteoblasts. Such a process depended on prostaglandin E2 (PGE2) and cyclooxygenase 2 (COX2). [53,54] Macrophages were also shown to release factors, such as lipoprotein receptor-related protein 1 (LRP1), that orchestrate the rejuvenation of bone repair.[55] Macrophages' critical role in bone repair was conclusively demonstrated by a complete failure in bone mineralization in fracture models depleted of macrophages.[5,12] Moreover, the macrophage polarization state also has a considerable influence over osteogenic differentiation. The phenotypes spectrum of

macrophages varies from the pro-inflammatory M1 macrophages, also known as classically activated macrophages, to the anti-inflammatory M2 macrophages, termed alternatively activated macrophages.[56] Following a fracture, M1 macrophages are responsible for mediating inflammation after tissue damage, while M2 macrophages have been shown to play a role in the later stages of bone remodeling.[57] The co-culture of macrophages with MSCs and HUVECs within liquefied microcapsules reinforced the importance of macrophages during bone osteogenesis. The MSCs, HUVECs, and macrophages culture ratio was set to 2:2:1. The MSCs and HUVECs ratio was previously tested within the liquefied capsules showing great results.[17,18] The amount of encapsulated macrophages was inspired by studies that show that the 2:1 ratio of MSCs co-cultured with macrophages was more favorable to osteogenic differentiation of MSCs.[58–60] In most conditions, the ALP activity was significantly higher in TRI microcapsules (**Figure 2c**). ALP is considered an early marker of osteoblastic differentiation.[37] Although ALP activity is only attributed to MSCs, our results indicated that macrophages could positively influence the osteogenic differentiation process. Interestingly, the presence of OCN, one of the most abundant proteins in the bone that is solely expressed and secreted by osteoblasts, was mostly observed in TRI microcapsules (**Figure 3b** and Figure S2d - Supporting Information).[38] The release of osteogenic cytokines, such as OPN, OPG, and BMP-2, also indicated that macrophages within the liquefied capsules affected osteogenesis (**Figure 3c-e**). In fact, macrophages were already shown to influence MSCs' ALP activity when incorporated in collagen-hydroxyapatite scaffolds, suggesting that macrophages themselves stimulate osteogenic differentiation.[59] However, there are no significant differences regarding the development of apatite-like minerals between CO and TRI microcapsules (**Figure 4**). Although the Osteoimage mineralization staining does not show huge differences between conditions and exhibits low mineralization (**Figure 4c**), when we cut the aggregates in half and observed the center by SEM-EDS, we detected an increased amount of crystals and mineralization (**Figure 4a**). The supplementation with osteogenic differentiation factors promoted the deposition of more P and Ca within the aggregates, but differences could not be noticed in the Ca/P ratio among conditions, although the values were similar to the native hydroxyapatite of the bone matrix.[41] Furthermore, no differences in hydroxyapatite expression were observed on the surface of aggregates (Figure S2e - Supporting Information). The mineralization ability of this encapsulation system was also studied after subcutaneous implantation in mice, and results from Alizarin and Masson's trichrome stainings show mineralized tissue even without *in vitro* pre-differentiation.[17] Although our results did not indicate differences, embedding macrophages in co-culture with MSCs in different types of scaffolds has been demonstrated to increase the mineralization of engineered tissues.[41,61–63]

Additionally, the co-culture of endothelial cells with stromal cells, as well as the mechanical stimulation added to microcapsules, have already proven to induce the deposition of new mineralized extracellular matrix.[18,25] We have previously encapsulated adipose-derived MSCs co-cultured with or without human osteoblasts under dynamic stimulation.[25] Although the fluid flow added to the culture system allowed the development of larger aggregates of cells and microparticles, as well as higher osteopontin expression and VEGF release, hydroxyapatite was only found in microcapsules encapsulating osteoblasts. Moreover, the number of primary human osteoblasts is limited, presenting a slow proliferation and long doubling time, making them unattractive for implantation.[64] Besides the ease of isolation, cell availability, immunocompatibility, and no donor site morbidity, such outcomes show another advantage of using umbilical cord-derived cells.

After evaluating the role of the macrophage on osteogenic stromal cell differentiation, we analyzed if macrophages could influence angiogenesis. VEGF release was significantly higher in TRI microcapsules for both basal and osteogenic media. Furthermore, when performing the endothelial tube formation assay with microcapsules supernatants, the number of segments, meshes, junctions, and the total segment length was superior in the same conditions. Such results indicate that encapsulated macrophages are closely connected with angiogenesis. Following ischemic injury, macrophages are essential for neovascularization and recuperation of blood flow (**Figure 5e**). Macrophages secrete several pro-inflammatory cytokines and chemokines, such as TNFs, interleukins, CSFs, C-X-C motif chemokine ligands (CXCLs), and C-C motif chemokine ligands (CCLs), for the recruitment of pro-angiogenic cells.[65] Besides the function of debris clearance, macrophages release matrix metalloproteinases (MMPs) to promote tissue remodeling.[66] Ultimately, macrophages guide the sprouting of new blood vessels and stimulate endothelial cell proliferation. The cellular sprouting occurs through the directed filopodia extension towards a higher VEGF concentration.[67] The paracrine signaling of different polarized macrophages may have different functions during the development of functional vascular channels. While M2a macrophages show to mediate the interactions between endothelial cells and pericytes, M2c macrophages appear to regulate sprouting, and M2f macrophages may regulate vessel maturation.[68] Moreover, M1 macrophages have been implicated in the release of VEGF during the initial stages of blood vessel formation, while M2a macrophages secrete platelet-derived growth factor-BB (PDGF-BB) to induce vascular anastomosis. M2c macrophages secrete high levels of MMP-9 and are involved in vascular remodeling.[69] Besides, Notch signaling plays a crucial role during angiogenesis through the crosstalk with VEGF receptors. Notch 1 and Hif-1α were shown to control macrophage recruitment and their interaction with endothelial cells during sprouting angiogenesis.[68,70,71]

Macrophages were also shown to stimulate endothelial tip cell fusion. In fact, the crosstalk between macrophages and VEGF induces vessel spouting and anastomosis, promoting vascular network formation.[72] Moreover, both MSCs and macrophages release VEGF.[69,73] The encapsulation of macrophages in different hydrogels showed similar outcomes.[74,75] For instance, implanting alginate-embedded macrophages in murine ischaemic hindlimb improved angiogenesis and arteriogenesis, leading to greater limb perfusion.[75] On the other hand, the co-culture of macrophages and endothelial cells in poly(ethylene glycol)-based hydrogels increased the vessel tubule volume, while macrophages changed their morphology in an endothelial cell-dependent manner.[74] Thus, we believe that upon implantation, the liquefied microcapsules can act as angiogenic inductors, stimulating the recruitment of the host vessels and promoting the vascularization and integration of the formed microtissues. Additionally, it is noteworthy that cytokines were detected and measured in the culture medium without destroying the microcapsules. Therefore, it implies that the measured growth factor released by the encapsulated cells was able to cross the multilayered membrane of microcapsules.

Besides the influence over osteogenesis and angiogenesis, the proposed liquefied microcapsules present immunomodulatory capabilities, allowed by the unique core environment and the semipermeable membrane, which can change the implantation paradigm. During bone healing, the polarization state acquired by macrophages can have a considerable influence over stromal cell differentiation.[76] After tissue damage, the inflammatory response is mediated mainly by pro-inflammatory M1 macrophages. Recently, Qiao *et al.* discovered that M1 macrophages are responsible for recruiting osteoblasts to the fracture site and inducing the proliferation of MSCs and endothelial cells.[77] The later stages of bone healing are mainly controlled by pro-healing M2 macrophages, which are responsible for the mineralization of the newly formed bone matrix as well as anastomosis of sprouting endothelial cells.[69,78] Considering the importance of the controlled and timely switch of macrophages between M1 and M2 phenotypes, we studied the plasticity of encapsulated macrophages by analyzing the cytokine profile of the microcapsules' microenvironment. The release of IL-1β, IL-6, and TNF-α is more associated with pro-inflammatory M1 macrophages. These pro-inflammatory cytokines are primarily detected at the early stage of bone healing and are suggested to be essential for MSCs recruitment and osteogenic differentiation.[79–81] Overall, the LegendPLEX panel detected the cytokines in the microcapsules supernatant after 7 days of culture. The release of IL-6 decreased over time for all liquefied microcapsules, while TNF-α was maintained constant (**Figure 6a-b**). The encapsulation of macrophages in the osteogenic medium led to the release of a higher amount of IL-1β compared to other conditions, although this quantity significantly decreased after 21 days (**Figure 6c**). The pro-healing cytokines, IL-10 and IL-1RA, mainly associated with anti-

inflammatory macrophage activation, were also detected after 7 and 21 days of culture.[82] The release of IL-10 was significantly higher in TRI microcapsules cultured in the osteogenic medium than in CO microcapsules (**Figure 6d**). The amount of this anti-inflammatory cytokine also increased after 21 days for TRI microcapsules. IL-10 was previously shown to inhibit osteoclast differentiation by acting directly on hemopoietic osteoclast precursors.[83] Additionally, IL-10 can give rise to a population of M2 macrophages.[56] IL-1RA release was also augmented in microcapsules incorporating macrophages, although it failed to reach significance in most conditions. IL-1RA is a natural inhibitor of the pro-inflammatory effect of IL-1β. [82] Moreover, the IL-6/IL-10 ratio decreased over time for all conditions. Decreased IL-6/IL-10 ratio is associated with better outcomes after trauma and can dictate the polarization state of encapsulated macrophages.[42] Although the difficulty in evaluating the encapsulated macrophages' phenotype individually, we can assume that undifferentiated macrophages presented an M1-like phenotype after 7 days of culture. Then, the variation of the cytokines profile indicated macrophages' polarization into an M2-like phenotype. The switch and balance of macrophages from M1 to M2 phenotypes were already observed in a mouse osteotomy model during endochondral ossification.[76] The microenvironment of CO microcapsules also shifted to a pro-healing state. The secretion of pro-inflammatory and pro-healing cytokines is not an exclusive function of macrophages. MSCs and endothelial cells were also shown to express these biomolecules, indicating that they function as immune regulators either by activating or suppressing immune cell function.[84,85] Additionally, the immunomodulatory capacity of MSCs is more than established and is highly associated with increased expression of immunosuppressive factors, such as IL-10.[86] Thus, engineered bone niches of CO and TRI microcapsules appear to drive the microenvironment pattern to a more pro-regenerative profile. However, it should be considered that the implantation of these microcapsules in an inflammatory environment can have a different effect. We can only claim that the undifferentiated macrophages in standard culture conditions within the liquefied microcapsules differentiate into a M2 phenotype. To overcome that issue, the surrounding microenvironment can be polarized by changing the last layer of microcapsules. Previously, we demonstrated that chitosan-ending capsules as well as the presence of MSCs, favor the balance of the surrounding macrophages toward a more regenerative profile through the up-regulation of anti-inflammatory markers and the release of pro-regenerative cytokines.[24] Furthermore, the delivery of macrophages has been shown promising to improve fracture healing. Recent *in vivo* studies have demonstrated that macrophages should be considered as a cell component when constructing biomaterials.[87,88]

The design of the biomaterial can dictate the host's immune response, as well as the response of incorporated cells. The incorporation of macrophages in 3D constructs has another crucial purpose: to facilitate the integration upon implantation. Encapsulated macrophages are able to recruit endothelial cells and fibroblasts to the implantation site.[13] When co-encapsulated in hydrogels with endothelial cells and fibroblasts, the presence of macrophages enhanced the organization of the extracellular matrix structure, revealing the importance of these immune cells in tissue remodeling and biomaterials integration.[89] Various researchers have focused on finding the best biomaterials' properties to initiate a favorable interaction with the host's macrophages by varying surface topography, charge, wettability, porosity, and ion release, among other characteristics.[14,90–92] The advantage of our encapsulation system over other technologies relies on its versatility. For instance, the proposed system can be set up with different core viscosities to modulate the cellular response of encapsulated MSCs through mechanotransduction pathways. Microparticles with different topographical features and stiffness cues can also be added to the liquefied core to modulate MSCs.[93,94] The last layer of the microcapsules can be altered to favor the host's macrophage polarization balance upon implantation.[24] The decoration of the last layer with bioinstructive signals (e.g., peptides or sugars) can be employed to improve biomaterials' integration.[95,96] Overall, the success of a certain biomaterial is mainly correlated with microenvironmental cues that can control immune responses toward healing and regeneration. Furthermore, the main advantage of the proposed technology is the presence of the multilayered membrane, which avoids the dispersion of the core contents to peripheral regions of the body after implantation, while the liquefied core confers the ability to adapt to structures with irregular shapes, such as tissue defects. Therefore, the proposed cell encapsulation system is an alternative to avoid the use the conventional scaffolds with fixed geometries and open surgery implantations while also allowing injection by minimally invasive procedures. This encapsulation system was already tested *in vivo*, and results showed that the blood vessels permeated the capsules and contributed to the gradual disruption of the multilayered membrane, while the encapsulated cells and microparticles remained grouped at the implantation site.[17] Importantly, we have already investigated the capability of this liquefied encapsulation system for long-term survival of several cell phenotypes, such as Wharton's jelly's MSCs, adipose-derived MSCs, primary human osteoblasts, L929 cell line, and human adipose microvascular endothelial cells, for up to 28 days in some cases.[17,18,23,25,97] Moreover, liquefied microcapsules can be combined with various fabrication methods to mimic the hierarchical structure and multiple length scales of native bone. 3D bioprinting offers unique prospects in this field. For future perspectives, the bioprinting of liquefied microcapsules could be considered for the generation of superior bone-

like tissues. The microsized liquefied pockets could wrap a functional environment for cell proliferation and differentiation, while the surrounding structure could act as a support, filling the bone defect. This strategy could overcome the cell anchorage-dependent issues as well as the lack of diffusion of nutrients and oxygen for cell survival.

Altogether, the present study demonstrated the role of macrophages in the production of bone-like microtissues when encapsulated within liquefied microcapsules. Incorporating these immune cells allowed to recreate the specific bone regenerative microenvironment within microcapsules and develop new microtissues with superior quality. Macrophages appear to be essential for osteogenic differentiation and promoting vascularization. We believe that the presented bioencapsulation strategy is a powerful self-regulated system, which might find great applicability in bone tissue engineering.

4. Conclusion

In summary, we got inspiration from the multiphenotypic cellular environment of bone tissue, where there is a crosstalk between osteoprogenitor cells and the immune system, to develop a method to fabricate biomimetic bone niche utilizing liquefied microcapsules. The concept relied on the co-culture of umbilical cord-derived cells, namely monocyte-derived macrophages, MSCs, HUVECs, and PCL microparticles within liquefied and semipermeable miniaturized reservoirs designed to drive self-regulated osteogenesis. The paracrine signaling between the three different cell phenotypes allowed fabricating bone-like microtissues, even in the absence of osteogenic differentiation factors. Furthermore, employing cells isolated from the umbilical cord tissue and blood determines the capacity of the engineered bone niche for personalized cell therapies. The use of autologous cells is attractive for tissue engineering strategies because it avoids a graft-versus-host immune response. Thus, we expect that our protocol might inspire a broader use of immune cells as a pro-regenerative component of implanted 3D tissue constructs. We envisage the use of engineered self-regulated microcapsules as an injectable system for bone repair or as elements in bottom-up tissue engineering assembly. Also, due to its strong modular character, the different elements can be adapted to fulfill the requirements of *in vitro* platforms for disease modeling and drug screening. We believe that after implantation, the liquefied microcapsules can stimulate vascularization and integration of the formed mineralized microtissues.

5. Experimental Section/Methods

Cells isolation from umbilical cord tissue and blood: Umbilical cord tissues were utilized to isolate MSCs and HUVECs. The umbilical cord blood was used to isolate monocytes. The

collected tissues were obtained under a cooperation agreement between the Aveiro Institute of Materials - University of Aveiro and Hospital de Aveiro (Aveiro, Portugal) after approval of the Competent Ethics Committee (CEC). The received human tissues were handled under the guidelines approved by the CEC. Informed consent was obtained from all subjects. Briefly, the umbilical cord tissue was transported in phosphate-buffered saline (PBS, Sigma-Aldrich) supplemented with 100 $U.mL^{-1}$ of penicillin and 0.1 $mg.mL^{-1}$ of streptomycin (PenStrep; ThermoFisher Scientific) and kept at 4 °C. For MSCs isolation[98], the umbilical cord tissue was washed with PBS and cut into 1 cm^2 segments. Umbilical cord vein and arteries were removed, and then the Wharton's jelly portion was isolated and reduced until obtaining an approximate diameter of 1-2 mm. Afterward, the pieces were transferred to Petri-dishes and maintained in α-MEM (minimum essential medium, Sigma-Aldrich) supplemented with 10% of heat-inactivated fetal bovine serum (FBS, ThermoFisher Scientific) and 100 $U.mL^{-1}$ of penicillin and 0.1 $mg.mL^{-1}$ of streptomycin. Petri-dishes were left undisturbed for 5-10 d at 37 °C in a humidified air atmosphere of 5% CO_2 until visible colonies of cells could be observed. For the isolation of HUVECs, the cord vein was filled with an enzymatic cocktail containing dispase II (Sigma-Aldrich) and collagenase type IV (Sigma-Aldrich). The cord was incubated at 37 ºC for 20 min. Afterward, the cells were collected and seeded in M199 growth medium (Sigma-Aldrich) and incubated in a humidified atmosphere of 5% CO_2 at 37ºC. After 4-6 h, the medium was changed to M199 supplemented with 20 % v/v umbilical cord blood serum, 2 mM L-glutamine (Gibco), 5 $ng.mL^{-1}$ Endothelial Cell Growth Supplement (ECGS, Sigma-Aldrich), 10 $\mu g.mL^{-1}$ heparin (PanReac AppliChem), 100 $U.mL^{-1}$ of penicillin and 0.1 $mg.mL^{-1}$ of streptomycin.[99,100] The blood was collected and transported using human umbilical cord blood collection bags (Macopharma). To obtain macrophages, monocytes were isolated from cord blood by centrifugation using Histopaque®-1077 (Sigma-Aldrich), followed by positive immunomagnetic separation with the human anti-CD14 purification kit (Miltenyi Biotec).[101] The purity of the separation was always confirmed by flow cytometry and was superior to 95% (Figure S1c - Supporting Information). Purified monocytes were differentiated *in vitro* into macrophages[69] in RPMI 1640 medium containing 10 % v/v FBS, 2 mM L-glutamine, 100 $U.mL^{-1}$ of penicillin and 0.1 $mg.mL^{-1}$ of streptomycin, and HEPES (10 mM, Gibco), and supplemented with 20 $ng.mL^{-1}$ of human M-CSF (Biolegend) for 5 d at 37 °C and 5% CO_2. The medium was renewed on the third day of culture. Positive controls were obtained by polarizing macrophages with 10 $ng.mL^{-1}$ of LPS (Lipopolysaccharides, Sigma-Aldrich) plus 100 $U.mL^{-1}$ of IFN-ϒ (Interferon ϒ, Biolegend) for M1 macrophages and with 20 $ng.mL^{-1}$ of IL-4 (Biolegend) plus 20 $ng.mL^{-1}$ of IL-13 (Biolegend) for M2 macrophages. Macrophages

were collected by gentle scraping after 48 h of polarization. Only freshly isolated cells were used.

Cell characterization: The phenotypic profiles of MSCs, HUVECs, monocytes, and monocyte-derived macrophages were assessed regarding mesenchymal (AF488-CD105, AF647-CD90, and PE-CD73, Biolegend), endothelial (APC-CD31, Biolegend), and monocyte/macrophage (AF647-CD14, AF488-CD16, AF488-CD80, AF647-CD163, APC-CD197, and FITC-CD206, Biolegend) markers before encapsulation. To analyze the surface markers, cells were detached from the culture flasks by incubation with TrypLE Express solution (Life Technologies) at 37 °C for 5 min. Then, cells were incubated with antibodies (5 µL of antibody per 1×10^6 of cells; 1 $mg.mL^{-1}$) for 45 min at 4 °C and in the dark. Samples were acquired and analyzed on a BD Accuri C6 Plus flow cytometer (BD Biosciences).

Poly(ϵ-caprolactone) microparticles production: PCL microparticles were produced by emulsion solvent evaporation technique, and the surface was functionalized with plasma treatment and collagen I, as similarly described in our previous report.[24] Briefly, a 5% w/v PCL (Mw ≈80 000, Merck) solution was prepared in methylene chloride (Honeywell). The PCL was slowly added to 0.5% w/v polyvinyl alcohol (PVA, Merck) solution and left stirring for 2 d at room temperature. Then, the microparticles were sieved to obtain a diameter range of 40–50 µm. Afterward, PCL microparticles were placed into a low-pressure plasma reactor chamber (ATTO, Diener Electronic) fitted with a radio frequency generator to induce the surface modification. Air was used as gas atmosphere. A low-pressure glow discharge was generated at 30 V and 0.2–0.4 mbar for 15 min. The microparticles were sterilized in 70 % of ethanol for 2 h. Ultimately, the microparticles were immersed in an acetic acid solution (20×10^{-3} M, Chem-Lab NV) containing collagen I (10 $\mu g.cm^{-2}$, rat protein tail, ThermoFisher Scientific) for 4 h at room temperature. The size of PCL microparticles was measured by ImageJ software.

Liquefied microcapsules fabrication: The different cell cultures were washed with PBS solution. Both MSCs and HUVECs were detached using Trypsin-EDTA (Merck). Macrophages were collected by gently scraping. MSCs and HUVECs (2.5×10^6 cells each per mL of alginate) with and without macrophages (1.25×10^6 cells per mL of alginate) were resuspended in low viscosity sodium alginate from brown algae (2.0% w/v, 9.5 cP, Merck), prepared in a buffer solution containing sodium chloride (0.15 M, NaCl, LabChem) and 2-(N-morpholino)ethanesulfonic acid hydrate (0.025 M, MES, Merck). Additionally, 30 mg mL^{-1} of PCL microparticles were added to the cells and alginate mix. Afterward, the microgels of

alginate, cells, and microparticles were generated by electrohydrodynamic atomization. For that, an external electrical field breaks the alginate jet containing cells and microparticles into fine droplets, followed by immediate crosslinking in a calcium chloride solution (0.1 M, $CaCl_2$, Merck) for approximately 20 min. Then, to build a multilayered membrane around the microgels, the layer-by-layer technique was employed by utilizing poly(L-lysine) (PLL, Mw≈30 000–70 000, Merck), alginate (ALG), and chitosan (CHT, NovaMatrix) as polyelectrolytes (0.3 $mg.mL^{-1}$, dissolved in the NaCl/MES buffer). The membrane contains 10 layers of polyelectrolytes. The liquefied core of microcapsules was obtained by chelation using ethylenediaminetetraacetic acid (2×10^{-3} M, EDTA, Merck) for 2 min at room temperature. We have previously observed that after capsules immersion in EDTA solution with different concentrations, namely 2×10^{-3} M, 5×10^{-3} M and 1×10^{-2} M, the cumulative calcium release increases with time. Different concentrations of EDTA resulted in similar calcium release profiles.[102] The pH of all solutions was set to 6.7, except for CHT, set to 6.3. All solutions were sterilized by filtration using a 0.22 μm filter. Two sets of microcapsules were generated for study purposes, namely a co-culture containing MSCs and HUVECs (CO microcapsules) and a tri-culture including macrophages (TRI microcapsules). Each encapsulation system was cultured in a combination of RPMI 1640 and M199 media, with (osteogenic) or without (basal) osteogenic differentiation supplementation. The osteogenic medium was obtained by supplementing the basal medium with ascorbic acid (50 $\mu g.ml^{-1}$, Merck), β-glycerophosphate (10 mM, Merck), and dexamethasone (10 mM, ACROS Organics). Microcapsules were cultured under a dynamic environment, utilizing spinner flasks (Celstir, Wheaton) with double sidearms at 50 rpm, for 21 d at 37 ºC and 5% CO_2. The diameter of microcapsules was measured by ImageJ software.

Lipophilic fluorescent labeling: To obtain the position of cells within the microcapsules, MSCs, HUVECs, and macrophages were stained with 3,3′-dioctadecyloxacarbocyanine perchlorate (DiO, ThermoFisher Scientific), 1,1′-dioctadecyl-3,3,3′,3′-tetramethylindodicarbocyanine, 4-chlorobenzenesulfonate salt (DiD, ThermoFisher Scientific), and 1,1′ -dioctadecyl-3,3,3′ ,3′-tetramethylindocarbocyanine perchlorate (DIL, ThermoFisher Scientific) lipophilic dyes, respectively. Prior to microcapsules generation, cells were resuspended in each dye solution diluted in PBS (1 mL of PBS containing 5 μL of dye per 1×10^6 cells) for 30 min at 37 °C. After 1 and 7 d post-encapsulation, samples were fixed in 4% w/v formaldehyde. Microcapsules were visualized by fluorescence microscopy (Axio Imager 2, Zeiss).

Live-Dead fluorescence assay: The viability of encapsulated cells was analyzed using the Live-Dead viability/cytotoxicity kit (ThermoFisher Scientific). After each time point, microcapsules were stained with calcein-AM (1:500 in PBS) and ethidium homodimer-1 (1:1000 in PBS) for 20 min at 37 °C, protected from light. Samples were washed with PBS and visualized by fluorescence microscopy (Axio Imager 2, Zeiss).

Mitochondrial metabolic activity quantification: The mitochondrial metabolic activity (MTS) quantification was performed using an MTS colorimetric assay (CellTiter96, AQueous One Solution Cell, Promega) according to the manufacturer's recommendation. Briefly, on days 1, 7, 14, and 21, microcapsules (n=50, in triplicate) were incubated with the reagent kit (1:6 in PBS) at 37 °C, 5% CO_2, protected from light. The absorbance was read after 4 h at a wavelength of 490 nm using a microplate reader (Gen 5, Synergy HT, Biotek).

DNA quantification: Double-stranded DNA quantification was performed according to the manufacturer's recommendation (Quant-iT PicoGreen dsDNA assay kit, Life Technologies) after cell lysis. Each sample (n=50, in triplicate) was suspended in 2% v/v of Triton X prepared in ultra-pure distilled water. After incubation for 1 h in a 37 °C shaking water bath, the samples were frozen at −80 °C until analysis. A standard curve provided by the kit was analyzed simultaneously with the samples. Samples and standards were incubated for 10 min at room temperature. Fluorescence was read at an excitation wavelength of 485/20 and 528/20 nm of emission, using a microplate reader (Gen 5, Synergy HT, Biotek).

Alkaline phosphatase activity quantification: After cell lysis, the alkaline phosphatase (ALP) activity was determined using the p-nitrophenol assay. The samples were lysed in the same way as in the previous step. A 0.2% w/v p-nytrophenyl phosphate (Sigma-Aldrich) substrate solution (pH = 9.8) was prepared in diethanolamine (1 M, Sigma-Aldrich). For ALP analysis, each sample (20 µL, in triplicate) was mixed with the substrate solution (60 µL) for 45 min at 37 °C protected from light. Then, the reaction was stopped (80 µL) with a stop solution (2 M NaOH and 0.2 mM EDTA). A standard curve was prepared by diluting p-nitrophenol solution (10 mM, Sigma-Aldrich) in the stop solution. The absorbance of samples and standards was read at 405 nm in a microplate reader (Gen 5 2.01, Synergy HT, Biotek).

Scanning electron microscopy (SEM): Microcapsules were washed with PBS, fixed in 4% w/v formaldehyde, and dehydrated in an increasing gradient series of ethanol. Then, samples were cut in half and fixed in a graphite stub (Ted Pella) with the inner part visible. After carbon

sputtering (K950X Turbo-Pumped Carbon Evaporator), the morphological evaluation of cells was visualized by SEM (accelerating voltage 15 kV, SEM Hitachi, SU-70 instrument).

Energy-dispersive x-ray spectroscopy (EDS): The chemical characterization of the extracellular matrix was carried out by an EDS detector (Bruker, Quantax 400 detector) coupled to the SEM. The peaks of calcium (Ca) and phosphorous (P) were determined by EDS spectra using Esprit software. The Ca/P ratio was calculated by deconvolution of Ca and P peaks after background subtraction.

Fluorescent staining of microcapsules content: The staining of microcapsules content was performed after 21 d of culture. For that, all samples were washed with PBS, fixed in 4% w/v formaldehyde, and permeabilized with 0.1% Triton X (Merck). Then, samples were incubated in 5% v/v of FBS for 1 h to block non-specific bindings. To analyze the F-actin network of cells and microcapsules structure, samples were incubated in Flash Phalloidin Red 594 (1 mg.mL^{-1}; 1:40 in PBS, Biolegend) for 45 min at 37 °C, and counterstaining with DAPI (1 mg.mL^{-1}; 1:1000 in PBS, ThermoFisher Scientific) for 5 min at room temperature. For the hydroxyapatite crystals assessment, samples were stained utilizing the OsteoImage™ Mineralisation Assay kit (Lonza) according to the manufacturer's instructions. Samples were counterstained with Flash Phalloidin Red 594 (1 mg.mL^{-1}; 1:40 in PBS, 45 min, 37 °C). For the immunofluorescence staining of OCN, OPN, and CD31, microcapsules were incubated overnight at 4 °C with the following primary antibodies: rabbit anti-human osteocalcin (1 mg.mL^{-1}; 1:100 in 5% FBS, Sigma-Aldrich), mouse anti-human osteopontin (1 mg.mL^{-1}; 1:200 in 5% FBS, Biolegend), and mouse anti-human CD31 (1 mg.mL^{-1}; 1:200 in 5% FBS, Biolegend). Samples were washed with PBS and incubated for 1 h at room temperature with the secondary antibodies: anti-rabbit Alexa-Fluor 647, anti-mouse Alexa-Fluor 647, and anti-mouse Alexa-Fluor 488 (1 mg.mL^{-1}; 1:500 in 5% FBS, ThermoFisher Scientific), respectively. Samples incubated only with the secondary antibody were used as controls. Ultimately, samples were counterstained with Flash Phalloidin Green 488 (1 mg.mL^{-1}; 1:40 in PBS, Biolegend, 45 min, 37 °C), Flash Phalloidin Red 594 (1 mg.mL^{-1}; 1:40 in PBS, 45 min, 37 °C), or DAPI (1 mg.mL^{-1}; 1:1000 in PBS, 5 min, room temperature). All stainings were visualized by fluorescence microscopy (Axio Imager 2, Zeiss).

Quantification of cytokines: The cytokines were detected and measured directly in the culture medium without destroying the microcapsules. Briefly, 1 mL of microcapsules were cultured in a spinner flask containing 20 mL of medium. 4 replicates were done for each condition. To

quantify the cytokines released by encapsulated cells, the supernatants of cultured microcapsules (1 mL) from different time points were stored at −80 °C until analysis. The amount of human vascular endothelial growth factor (VEGF) was detected using a commercially available VEGF kit (Abcam) according to the manufacturer's specifications. The absorbance was read at 450 nm in a microplate reader (Gen 5, Synergy HT, Biotek). The LEGENDplex Human Bone Metabolism Panel and the Human M1/M2 Macrophage Panel (Biolegend) were utilized according to the manufacturer's specifications to detect the other cytokines. The samples were acquired on a BD Accuri C6 Plus flow cytometer (BD Biosciences) and analyzed using the BioLegend's LEGENDplex Data Analysis Software v8.

Tube formation assay: The endothelial cell tube formation assay[103] was determined utilizing μ-slide angiogenesis (ibidi). Briefly, Matrigel (Corning) was thawed and added to each well according to the manufacturer's instructions. After polymerization of the gel, 1 x 10^4 HUVECs were seeded per well with the supernatants of microcapsules collected 21 d post-encapsulation. M199 completed medium was utilized as a control. After 6 h, the tube formation was visible, and cells were stained with calcein-AM (1 $mg.mL^{-1}$; 1:500 in PBS) for 20 min at 37 °C, protected from light. Cells were visualized by fluorescence microscopy (Axio Imager 2, Zeiss). The number of tubes and tube length were evaluated using the Angiogenesis Analyzer (ImageJ software).

Statistical analysis: Statistical analysis was performed using one-way and two-way analysis of variance (ANOVA) with Tukey's post-hoc test (Graph-Pad Prism 9.0.0). p-values<0.05 were considered statistically significant (****p<0.001; ***p<0.001; **p<0.01; *p<0.05). All results were presented as mean ± standard deviation.

Acknowledgements

S. Nadine acknowledges the financial support given by the Portuguese Foundation for Science and Technology (FCT) with the doctoral grant of Sara Nadine (SFRH/BD/130194/2017). This work was financed by national funds (OE) through FCT in the scope of the projects "TETRISSUE" (PTDC/BTM-MAT/3201/2020), "CIRCUS" (PTDC/BTM-MAT/31064/2017), and "MIMETIc" (PTDC/BTM-MAT/31210/2017) and the European Research Council for project "ATLAS" (ERC-2014-AdG-669858). “CIRCUS” and “MIMETIc” are also supported by the Programa Operacional Competitividade e Internacionalização, in the component FEDER (POCI-01-0145-FEDER-031064 and POCI-01-0145-FEDER-031210). S. G. Patrício acknowledges the individual contract 2020.00366.CEECIND. This work was developed within

the scope of the project CICECO-Aveiro Institute of Materials, UIDB/50011/2020, UIDP/50011/2020 & LA/P/0006/2020, financed by national funds through the FCT/MCTES.

References

[1] C. R. Correia, S. Nadine, J. F. Mano, C. R. Correia, S. Nadine, J. F. Mano, *Adv. Funct. Mater.* **2020**, *30*, 1908061.

[2] H. Takayanagi, *Nat. Rev. Immunol.* **2007**, *7*, 292.

[3] A. Longoni, L. Knežević, K. Schepers, H. Weinans, A. J. W. P. Rosenberg, D. Gawlitta, *npj Regen. Med.* **2018**, *3*, 22.

[4] J. Pajarinen, T. Lin, E. Gibon, Y. Kohno, M. Maruyama, K. Nathan, L. Lu, Z. Yao, S. B. Goodman, *Biomaterials* **2019**, *196*, 80.

[5] K. A. Alexander, M. K. Chang, E. R. Maylin, T. Kohler, R. Müller, A. C. Wu, N. Van Rooijen, M. J. Sweet, D. A. Hume, L. J. Raggatt, A. R. Pettit, *J. Bone Miner. Res.* **2011**, *26*, 1517.

[6] L. Batoon, S. M. Millard, M. E. Wullschleger, C. Preda, A. C. K. Wu, S. Kaur, H. W. Tseng, D. A. Hume, J. P. Levesque, L. J. Raggatt, A. R. Pettit, *Biomaterials* **2019**, *196*, 51.

[7] Y. Niu, Z. Wang, Y. Shi, L. Dong, C. Wang, *Bioact. Mater.* **2021**, *6*, 244.

[8] M. K. Chang, L.-J. Raggatt, K. A. Alexander, J. S. Kuliwaba, N. L. Fazzalari, K. Schroder, E. R. Maylin, V. M. Ripoll, D. A. Hume, A. R. Pettit, *J. Immunol.* **2008**, *181*, 1232.

[9] V. Nicolaidou, M. M. Wong, A. N. Redpath, A. Ersek, D. F. Baban, L. M. Williams, A. P. Cope, N. J. Horwood, *PLoS One* **2012**, *7*, DOI 10.1371/JOURNAL.PONE.0039871.

[10] F. Loi, L. A. Córdova, R. Zhang, J. Pajarinen, T. H. Lin, S. B. Goodman, Z. Yao, *Stem Cell Res. Ther.* **2016**, *7*, 1.

[11] K. Németh, A. Leelahavanichkul, P. S. T. Yuen, B. Mayer, A. Parmelee, K. Doi, P. G. Robey, K. Leelahavanichkul, B. H. Koller, J. M. Brown, X. Hu, I. Jelinek, R. A. Star, É. Mezey, *Nat. Med.* **2009**, *15*, 42.

[12] L. J. Raggatt, M. E. Wullschleger, K. A. Alexander, A. C. K. Wu, S. M. Millard, S. Kaur, M. L. Maugham, L. S. Gregory, R. Steck, A. R. Pettit, *Am. J. Pathol.* **2014**, *184*, 3192.

[13] C. Dollinger, S. Ciftci, H. Knopf-Marques, R. Guner, A. M. Ghaemmaghami, C. Debry, J. Barthes, N. E. Vrana, *J. Tissue Eng. Regen. Med.* **2018**, *12*, 330.

[14] Z. Chen, T. Klein, R. Z. Murray, R. Crawford, J. Chang, C. Wu, Y. Xiao, *Mater. Today* **2016**, *19*, 304.

[15] K. G. Battiston, J. W. C. Cheung, D. Jain, J. P. Santerre, *Biomaterials* **2014**, *35*, 4465.

[16] M. Grellier, P. L. Granja, J. C. Fricain, S. J. Bidarra, M. Renard, R. Bareille, C. Bourget, J. Amédée, M. A. Barbosa, *Biomaterials* **2009**, *30*, 3271.

[17] C. R. Correia, T. C. Santos, R. P. Pirraco, M. T. Cerqueira, A. P. Marques, R. L. Reis, J. F. Mano, *Acta Biomater.* **2017**, *53*, 483.

[18] C. R. Correia, R. P. Pirraco, M. T. Cerqueira, A. P. Marques, R. L. Reis, J. F. Mano, *Sci. Rep.* **2016**, *6*, 21883.

[19] C. Huang, V. P. Ness, X. Yang, H. Chen, J. Luo, E. B. Brown, X. Zhang, *J. Bone Miner. Res.* **2015**, *30*, 1217.

[20] A. Grosso, M. G. Burger, A. Lunger, D. J. Schaefer, A. Banfi, N. Di Maggio, *Front. Bioeng. Biotechnol.* **2017**, *5*, 68.

[21] D. Lopes, C. Martins-Cruz, M. B. Oliveira, J. F. Mano, *Biomaterials* **2018**, *185*, 240.

[22] C. R. Correia, S. Gil, R. L. Reis, J. F. Mano, *Adv. Healthc. Mater.* **2016**, *5*, 1346.

[23] C. R. Correia, R. L. Reis, J. F. Mano, *Biomacromolecules* **2013**, *14*, 743.

[24] S. Nadine, C. R. Correia, J. F. Mano, *Adv. Healthc. Mater.* **2021**, *10*, 2001993.

[25] S. Nadine, S. G. Patrício, C. R. Correia, J. F. Mano, *Biofabrication* **2019**, *12*, 15005.

[26] S. Nadine, S. G. Patrício, C. C. Barrias, I. S. Choi, M. Matsusaki, C. R. Correia, J. F. Mano, *Adv. Biosyst.* **2020**, *4*, 2000127.

[27] A. Bongso, C. Y. Fong, *Stem Cell Rev. Reports* **2013**, *9*, 226.

[28] I. Arutyunyan, T. Fatkhudinov, G. Sukhikh, *Stem Cell Res. Ther.* **2018**, *9*, 236.

[29] S. Tipnis, C. Viswanathan, A. S. Majumdar, *Immunol. Cell Biol.* **2010**, *88*, 795.

[30] M. L. Weiss, C. Anderson, S. Medicetty, K. B. Seshareddy, R. J. Weiss, I. VanderWerff, D. Troyer, K. R. McIntosh, *Stem Cells* **2008**, *26*, 2865.

[31] L. L. Liau, B. H. I. Ruszymah, M. H. Ng, J. X. Law, *Curr. Res. Transl. Med.* **2020**, *68*, 5.

[32] A. Gupta, S. F. El-Amin, H. J. Levy, R. Sze-Tu, S. E. Ibim, N. Maffulli, *J. Orthop. Surg. Res.* **2020**, *15*, 49.

[33] D. N. Heo, M. Hospodiuk, I. T. Ozbolat, *Acta Biomater.* **2019**, *95*, 348.

[34] R. C. Gonçalves, A. Banfi, M. B. Oliveira, J. F. Mano, *Biomaterials* **2021**, *269*, 120628.

[35] T. J. Fernandes, J. M. Hodge, P. P. Singh, D. G. Eeles, F. M. Collier, I. Holten, P. R. Ebeling, G. C. Nicholson, J. M. W. Quinn, *PLoS One* **2013**, *8*, e73266.

[36] V. M. Gaspar, P. Lavrador, J. Borges, M. B. Oliveira, J. F. Mano, *Adv. Mater.* **2020**,

32, 1903975.

[37] H. Orimo, *J. Nippon Med. Sch.* **2010**, *77*, 4.

[38] M. L. Zoch, T. L. Clemens, R. C. Riddle, *Bone* **2016**, *82*, 42.

[39] N. Udagawa, N. Takahashi, H. Yasuda, A. Mizuno, K. Itoh, Y. Ueno, T. Shinki, M. T. Gillespie, T. J. Martin, K. Higashio, T. Suda, *Endocrinology* **2000**, *141*, 3478.

[40] K. Tsuji, A. Bandyopadhyay, B. D. Harfe, K. Cox, S. Kakar, L. Gerstenfeld, T. Einhorn, C. J. Tabin, V. Rosen, *Nat. Genet.* **2006**, *38*, 1424.

[41] V. S. Kattimani, S. Kondaka, K. P. Lingamaneni, *https://doi.org/10.4137/BTRI.S36138* **2016**, *7*, BTRI.S36138.

[42] H. B. Sapan, I. Paturusi, I. Jusuf, I. Patellongi, M. N. Massi, A. D. Pusponegoro, S. K. Arief, I. Labeda, A. A. Islam, L. Rendy, M. Hatta, *Int. J. Burns Trauma* **2016**, *6*, 37.

[43] M. Ansari, *Prog. Biomater.* **2019**, *8*, 223.

[44] N. Annabi, A. Tamayol, J. A. Uquillas, M. Akbari, L. E. Bertassoni, C. Cha, G. Camci-Unal, M. R. Dokmeci, N. A. Peppas, A. Khademhosseini, *Adv. Mater.* **2014**, *26*, 85.

[45] Y. Wu, S. Joseph, N. R. Aluru, *J. Phys. Chem. B* **2009**, *113*, 3512.

[46] O. Jeon, C. Powell, S. M. Ahmed, E. Alsberg, *Tissue Eng. Part A* **2010**, *16*, 2915.

[47] C. R. Correia, M. Ghasemzadeh-Hasankolaei, J. F. Mano, *PLoS One* **2019**, *14*, e0218045.

[48] S. Duggal, K. B. Frønsdal, K. Szöke, A. Shahdadfar, J. E. Melvik, J. E. Brinchmann, *https://home.liebertpub.com/tea* **2008**, *15*, 1763.

[49] M. Westhrin, M. Xie, M. Olderøy, P. Sikorski, B. L. Strand, T. Standal, *PLoS One* **2015**, *10*, e0120374.

[50] M. Juhas, N. Abutaleb, J. T. Wang, J. Ye, Z. Shaikh, C. Sriworarat, Y. Qian, N. Bursac, *Nat. Biomed. Eng.* **2018**, *2*, 942.

[51] M. R. Borrelli, M. S. Hu, W. X. Hong, J. D. Oliver, D. Duscher, M. T. Longaker, H. P. Lorenz, *J. Craniofac. Surg.* **2019**, *30*, 2640.

[52] L. S. Saleh, M. Carles-Carner, S. J. Bryant, *Acta Biomater.* **2018**, *71*, 37.

[53] V. Nicolaidou, M. M. Wong, A. N. Redpath, A. Ersek, D. F. Baban, L. M. Williams, A. P. Cope, N. J. Horwood, *PLoS One* **2012**, *7*, DOI 10.1371/JOURNAL.PONE.0039871.

[54] P. Guihard, Y. Danger, B. Brounais, E. David, R. Brion, J. Delecrin, C. D. Richards, S. Chevalier, F. Rédini, D. Heymann, H. Gascan, F. Blanchard, *Stem Cells* **2012**, *30*, 762.

[55] L. Vi, G. S. Baht, E. J. Soderblom, H. Whetstone, Q. Wei, B. Furman, V. Puviindran, P. Nadesan, M. Foster, R. Poon, J. P. White, Y. Yahara, A. Ng, T. Barrientos, M. Grynpas, M. A. Mosely, B. A. Alman, *Nat. Commun.* **2018**, *9*, 5191.

[56] D. M. Mosser, J. P. Edwards, *Nat. Rev. Immunol. 2008 812* **2008**, *8*, 958.

[57] C. Schlundt, H. Fischer, C. H. Bucher, C. Rendenbach, G. N. Duda, K. Schmidt-Bleek, *Acta Biomater.* **2021**, *133*, 46.

[58] B. Zhang, M. Zhang, Y. Sun, M. Li, F. Han, C. Wu, *Prog. Nat. Sci. Mater. Int.* **2021**, *31*, 883.

[59] R. Sridharan, K. J. Genoud, D. J. Kelly, F. J. O'Brien, *ACS Appl. Bio Mater.* **2020**, *3*, 7562.

[60] B. Zhang, F. Han, Y. Wang, Y. Sun, M. Zhang, X. Yu, C. Qin, H. Zhang, C. Wu, B. Zhang, F. Han, Y. Wang, Y. Sun, M. Zhang, X. Yu, C. Qin, H. Zhang, C. Wu, *Adv. Sci.* **2022**, 2200670.

[61] D. A. Cantu, P. Hematti, W. J. Kao, *Stem Cells Transl. Med.* **2012**, *1*, 740.

[62] X. T. He, R. X. Wu, X. Y. Xu, J. Wang, Y. Yin, F. M. Chen, *Acta Biomater.* **2018**, *71*, 132.

[63] M. Romero-López, Z. Li, C. Rhee, M. Maruyama, J. Pajarinen, B. O'Donnell, T. H. Lin, C. W. Lo, J. Hanlon, R. Dubowitz, Z. Yao, B. A. Bunnell, H. Lin, R. S. Tuan, S. B. Goodman, *Tissue Eng. - Part A* **2020**, *26*, 1099.

[64] S. Zhu, S. Ehnert, M. Rouß, V. Häussling, R. H. Aspera-Werz, T. Chen, A. K. Nussler, *Int. J. Mol. Sci.* **2018**, *19*, DOI 10.3390/IJMS19082284.

[65] Z. Szekanecz, A. E. Koch, *Nat. Clin. Pract. Rheumatol.* **2007**, *3*, 635.

[66] T. A. Wynn, K. M. Vannella, *Immunity* **2016**, *44*, 450.

[67] L. Jakobsson, C. A. Franco, K. Bentley, R. T. Collins, B. Ponsioen, I. M. Aspalter, I. Rosewell, M. Busse, G. Thurston, A. Medvinsky, S. Schulte-Merker, H. Gerhardt, *Nat. Cell Biol.* **2010**, *12*, 943.

[68] P. L. Graney, S. Ben-Shaul, S. Landau, A. Bajpai, B. Singh, J. Eager, A. Cohen, S. Levenberg, K. L. Spiller, *Sci. Adv.* **2020**, *6*, eaay6391.

[69] K. L. Spiller, R. R. Anfang, K. J. Spiller, J. Ng, K. R. Nakazawa, J. W. Daulton, G. Vunjak-Novakovic, *Biomaterials* **2014**, *35*, 4477.

[70] T. Tammela, G. Zarkada, H. Nurmi, L. Jakobsson, K. Heinolainen, D. Tvorogov, W. Zheng, C. A. Franco, A. Murtomäki, E. Aranda, N. Miura, S. Ylä-Herttuala, M. Fruttiger, T. Mäkinen, A. Eichmann, J. W. Pollard, H. Gerhardt, K. Alitalo, *Nat. Cell Biol.* **2011**, *13*, 1202.

[71] C. Gerri, R. Marín-Juez, M. Marass, A. Marks, H.-M. Maischein, D. Y. R. Stainier, *Nat. Commun.* **2017**, *8*, 15492.

[72] A. Fantin, J. M. Vieira, G. Gestri, L. Denti, Q. Schwarz, S. Prykhozhij, F. Peri, S. W. Wilson, C. Ruhrberg, *Blood* **2010**, *116*, 829.

[73] L. Chen, E. E. Tredget, P. Y. G. Wu, Y. Y. G. Wu, *PLoS One* **2008**, *3*, 1886.

[74] E. M. Moore, G. Ying, J. L. West, *Adv. Biosyst.* **2017**, *1*, 1600021.

[75] F. E. Ludwinski, A. S. Patel, G. Damodaran, J. Cho, J. Furmston, Q. Xu, S. N. Jayasinghe, A. Smith, B. Modarai, *npj Regen. Med.* **2019**, *4*, 6.

[76] C. Schlundt, T. El Khassawna, A. Serra, A. Dienelt, S. Wendler, H. Schell, N. van Rooijen, A. Radbruch, R. Lucius, S. Hartmann, G. N. Duda, K. Schmidt-Bleek, *Bone* **2018**, *106*, 78.

[77] W. Qiao, H. Xie, J. Fang, J. Shen, W. Li, D. Shen, J. Wu, S. Wu, X. Liu, Y. Zheng, K. M. C. Cheung, K. W. K. Yeung, *Biomaterials* **2021**, *276*, 121038.

[78] Y. Zhang, T. Böse, R. E. Unger, J. A. Jansen, C. J. Kirkpatrick, J. J. J. P. van den Beucken, *Cell Tissue Res.* **2017**, *369*, 273.

[79] M. L. Olmedo, P. S. Landry, K. K. Sadasivan, J. A. Albright, W. D. Meek, R. Routh, A. A. Marino, *J. Orthop. Trauma* **1999**, *13*, 356.

[80] G. E. Glass, J. K. Chan, A. Freidin, M. Feldmann, N. J. Horwood, J. Nanchahal, *Proc. Natl. Acad. Sci. U. S. A.* **2011**, *108*, 1585.

[81] X. Yang, B. F. Ricciardi, A. Hernandez-Soria, Y. Shi, N. Pleshko Camacho, M. P. G. Bostrom, *Bone* **2007**, *41*, 928.

[82] A. MANTOVANI, A. SICA, S. SOZZANI, P. ALLAVENA, A. VECCHI, M. LOCATI, *Trends Immunol.* **2004**, *25*, 677.

[83] M. H. Hong, H. Williams, C. H. Jin, J. W. Pike, *J. Bone Miner. Res.* **2000**, *15*, 911.

[84] D. Kyurkchiev, *World J. Stem Cells* **2014**, *6*, 552.

[85] J. Mai, A. Virtue, J. Shen, H. Wang, X.-F. Yang, *J. Hematol. Oncol.* **2013**, *6*, 61.

[86] L. Müller, A. Tunger, M. Wobus, M. von Bonin, R. Towers, M. Bornhäuser, F. Dazzi, R. Wehner, M. Schmitz, *Front. Cell Dev. Biol.* **2021**, *9*, DOI 10.3389/fcell.2021.637725.

[87] J. M. Živković, S. T. Stojanović, M. Đ. Vukelić-Nikolić, M. B. Radenković, J. G. Najdanović, M. Ćirić, S. J. Najman, *Int. Orthop.* **2021**, *45*, 1087.

[88] M. Kang, G. Thalji, C.-C. Huang, S. Shirazi, Y. Lu, S. Ravindran, L. F. Cooper, *Front. cell Dev. Biol.* **2020**, *8*, 596622.

[89] J. Barthes, C. Dollinger, C. B. Muller, U. Liivas, A. Dupret-Bories, H. Knopf-Marques, N. E. Vrana, *Front. Bioeng. Biotechnol.* **2018**, *6*, DOI 10.3389/fbioe.2018.00108.

[90] Y. Niu, Q. Li, R. Xie, S. Liu, R. Wang, P. Xing, Y. Shi, Y. Wang, L. Dong, C. Wang, *Biomaterials* **2017**, *139*, 39.

[91] J. Barthes, P. Lagarrigue, V. Riabov, G. Lutzweiler, J. Kirsch, C. Muller, E. J. Courtial, C. Marquette, F. Projetti, J. Kzhyskowska, P. Lavalle, N. E. Vrana, A. Dupret-Bories,

Biomaterials **2021**, *268*, 120549.

[92] G. Vallés, F. Bensiamar, L. Crespo, M. Arruebo, N. Vilaboa, L. Saldaña, *Biomaterials* **2015**, *37*, 124.

[93] I. M. Bjørge, M. Salmeron-Sanchez, C. R. Correia, J. F. Mano, *Small* **2020**, *16*, 2001975.

[94] C. R. Correia, J. Gaifem, M. B. Oliveira, R. Silvestre, J. F. Mano, *Biomater. Sci.* **2017**, *5*, 551.

[95] J. Borges, J. F. Mano, *Chem. Rev.* **2014**, *114*, 8883.

[96] C. R. Correia, I. M. Bjørge, J. Zeng, M. Matsusaki, J. F. Mano, *Adv. Healthc. Mater.* **2019**, *8*, 1901221.

[97] S. Vilabril, S. Nadine, C. M. S. S. Neves, C. R. Correia, M. G. Freire, J. A. P. Coutinho, M. B. Oliveira, J. F. Mano, *Adv. Healthc. Mater.* **2021**, *10*, 2100266.

[98] A. Petsa, S. Gargani, A. Felesakis, N. Grigoriadis, I. Grigoriadis, *Vitr. Cell. Dev. Biol. - Anim.* **2009**, *45*, 573.

[99] A. S. Silva, L. F. Santos, M. C. Mendes, J. F. Mano, *Biomaterials* **2020**, *231*, 119664.

[100] B. Baudin, A. Bruneel, N. Bosselut, M. Vaubourdolle, *Nat. Protoc.* **2007**, *2*, 481.

[101] M. C. Nielsen, M. N. Andersen, H. J. Møller, *Immunology* **2020**, *159*, 63.

[102] C. R. Correia, P. Sher, R. L. Reis, J. F. Mano, *Soft Matter* **2013**, *9*, 2125.

[103] I. Arnaoutova, H. K. Kleinman, *Nat. Protoc.* **2010**, *5*, 628.

S. Nadine, I. Fernandes, Dr. S. G. Patrício, Dr. C. R. Correia*, Prof. J. F. Mano*

Liquefied microcapsules compartmentalizing macrophages and umbilical cord-derived cells for bone tissue engineering

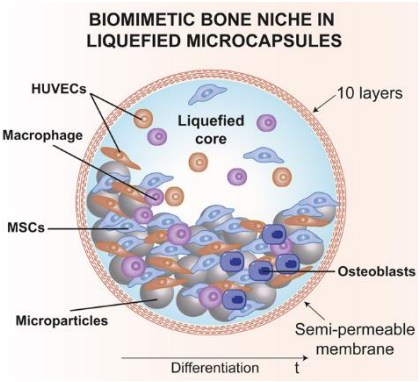

Liquefied and semipermeable miniaturized reservoirs are co-cultured with umbilical cord-derived cells, namely monocyte-derived macrophages, mesenchymal-derived stromal cells, and human umbilical vein endothelial cells, to bioengineer biomimetic bone niches. The multilayered membrane permits the diffusion of essential molecules for cell survival, while the microparticles within the liquefied core act as anchorage sites for cell adhesion, proliferation, and differentiation.

Supporting Information

Liquefied microcapsules compartmentalizing macrophages and umbilical cord-derived cells for bone tissue engineering

Sara Nadine, Inês Fernandes, Sónia G. Patrício, Clara R. Correia, João F. Mano**

Figure S1. Flow cytometry analysis of human mesenchymal-derived stem cells (MSCs), human umbilical vein endothelial cells (HUVECs), monocytes, and monocytes-derived macrophages, after isolation from the umbilical cord tissue and blood (n=3).

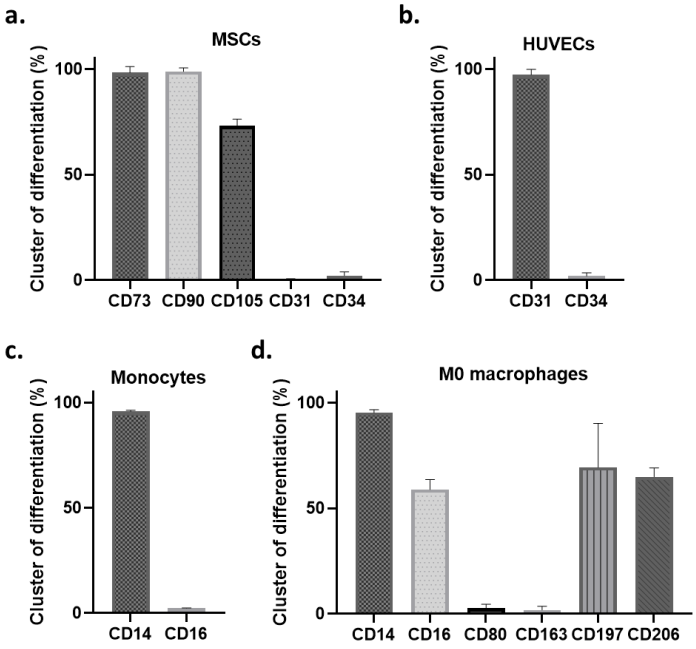

Figure S2. (a-c) OPN, OPG, and BMP-2 protein release measured by LegendPLEX Human Bone Metabolism Panel of CO and TRI microcapsules cultured for 7 days in basal and

osteogenic media (n=4). (d) Semi-quantitative analysis of OCN in CO and TRI microcapsules cultured in basal and osteogenic media for 21 (n=5). OCN stained area was calculated from thresholded images using ImageJ software and normalized per number of nuclei. (e) Semi-quantitative analysis of hydroxyapatite in CO and TRI microcapsules cultured in basal and osteogenic media for 21 (n=4) using OsteoImage staining images. Hydroxyapatite stained area was calculated from thresholded images using ImageJ software and normalized per area of aggregate (ECM area). *p*-values<0.05 were considered statistically significant.

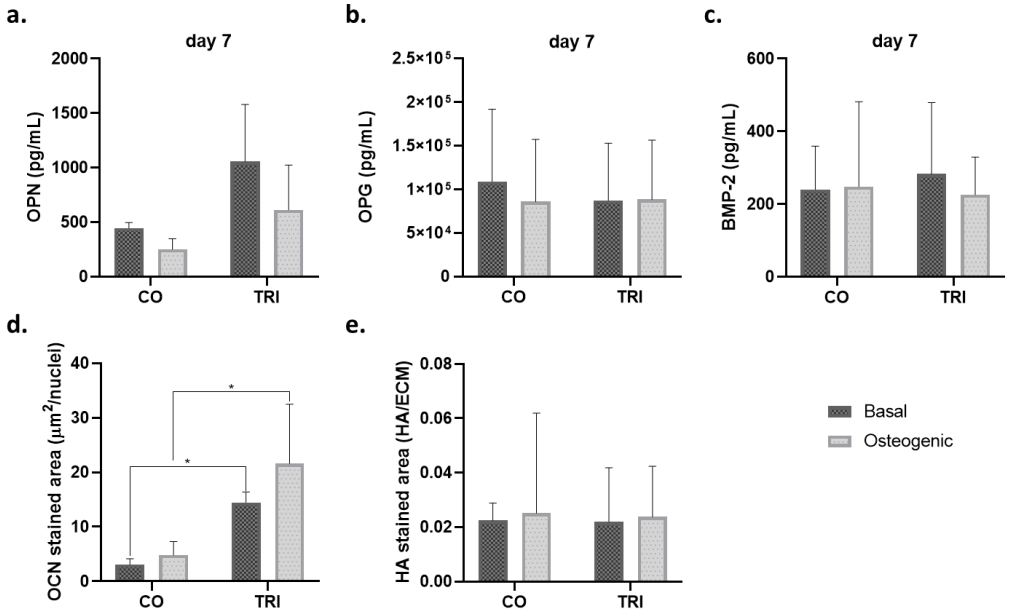

Figure S3. Representative microscopic images of the endothelial tube formation assay incubated with supernatants of microcapsules (basal condition).

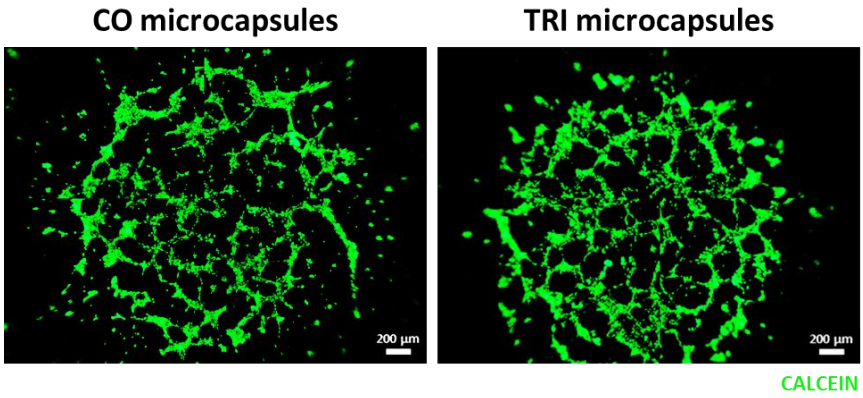

Figure S4. Cell proliferation assay determined by DNA quantification of CO and TRI microcapsules cultured up to 21 days in basal and osteogenic media. *p*-values<0.05 were considered statistically significant.